Review

A Review on Ultrafast Laser Microwelding of Transparent Materials and Transparent Material–Metals

Jiayi Xu [1,†], Qing Jiang [1,†], Jin Yang [1,*], Jiangmei Cui [2], Yixuan Zhao [1], Min Zheng [3], J. P. Oliveira [4], Zhi Zeng [5,*], Rui Pan [6] and Shujun Chen [6]

1   School of Materials Engineering, Shanghai University of Engineering Science, Shanghai 201620, China
2   School of Materials and Environmental Engineering, Chengdu Technological University, Chengdu 610031, China
3   School of Advanced Manufacturing, Nanchang University, Nanchang 330031, China
4   CENIMAT|i3N, Department of Materials Science, School of Science and Technology, NOVA University Lisbon, 2829-516 Caparica, Portugal
5   School of Mechanical and Electronic Engineering, University of Electronic Science and Technology of China, Chengdu 611731, China
6   Faculty of Materials and Manufacturing, Beijing University of Technology, Beijing 100124, China
*   Correspondence: jyang@sues.edu.cn (J.Y.); zhizeng@uestc.edu.cn (Z.Z.)
†   These authors contributed equally to this work.

Abstract: Transparent hard and brittle (THB) materials have generated significant interest due to their excellent properties, such as wide spectral transmittance, heat resistance, chemical inactivity and high mechanical strength. To further explore the application of THB materials, it is inevitable to be confronted with a range of joining THB materials and THB material–metals. Ultrafast (UF) laser microwelding enables a new means of joining THB materials and THB material–metals, due to a localized energy deposition method, which is dominated by nonlinear absorption. This process can realize high-quality micro-zone direct joining of THB materials or THB material–metals without the assistance of a light-absorbing intermediate layer. In this paper, we review the advances in UF laser microwelding of THB materials and THB material–metals considering the last two decades, from the analysis of the interaction mechanism between UF laser and matter to the key influencing factors and practical applications of this technology. Finally, the existing problems and the future research focus of UF laser microwelding technology of THB materials and THB material–metals are discussed.

Keywords: ultrafast laser; laser welding; transparent hard and brittle materials; metals; nonlinear absorption

1. Introduction

Transparent dielectric materials, such as glasses, optical crystals and sapphires, despite their inherent brittleness and susceptibility to mechanical shocks and stresses, exhibit excellent properties, such as wide spectral transmittance, heat resistance, chemical inactivity and high mechanical strength [1] and have generated significant interest in the field of optics, aerospace, communications and electronics [2–5]. However, in practical applications of these transparent hard and brittle (THB) materials, researchers are confronted with a range of joining processes for homogeneous and heterogeneous materials (i.e., THB material–THB materials and THB material–metals). Taking joining of THB material–metals as an example, given that metals have superior machinability, ductility and high compression strength, THB material–metal hybrid components find multiple potential applications in photovoltaic devices, optical windows for weapons and equipment, and vacuum-sealed connectors [6,7]. A variety of conventional technologies for joining THB materials have been attempted including adhesive bonding [8], anodic bonding [9], solid-state bonding [10], brazing [11] and fusion welding [5]. Nevertheless, most of these methods have intrinsic limitations

and shortcomings in offering reliable, solid bonds, such as contamination and aging of the binding agent, thermal mismatch, low accuracy and the necessity for high-temperature heating, which adversely impact the component performance and its operational lifetime.

Laser microwelding can deliver laser energy exactly into the interface of welded components without any physical contact, eventually obtaining a solid bonding of the materials [12,13]. However, traditional transmission laser welding has a notable drawback in joining THB materials, which is the necessity for light-absorbing intermediate layers, especially when joining two THB materials. Since THB materials exhibit transparency in the visible (VIS) to near-infrared (NIR) spectrum, which are common wavelengths used during the laser-based process, the efficiency of laser energy deposition is extremely low, which makes traditional laser welding technologies unable to join THB materials without the assistance of a light-absorbing intermediate layer [14]. Ultrafast (UF) laser technology can trigger linear absorption in the opaque material and nonlinear absorption in the THB material due to the extremely high peak intensity, causing a variety of processes, including melting, ablation and solidification [7,15]. This method enables a direct welding of THB materials or THB material–metals without the need for any fillers [16]. Additionally, Ozeki et al. [17] demonstrated that glass–copper welding with an fs-pulse required less energy and led to a thinner heat affected zone (HAZ) compared to that with a ns-pulse. On the one hand, an attenuated HAZ with the use of an UF laser reduces the possibility of uneven heating and eliminates the resultant high thermal gradient. Upon material cooling, the high thermal gradient is prone to translate to high stress gradients, which can be responsible for the formation of weld microcracks [18]. On the other hand, it also allows the prepared component to preserve its high transparency, as well as the optical transmission efficiency of the base materials during welding, due to the severe restriction of the modified region, which is critical for industrial applications of THB material-based components. Hence, UF laser technology has opened up a new way for the microwelding of THB materials and THB material–metals.

UF laser microwelding technology has developed rapidly in recent years, providing the required joint performances [19–23]. The application of this technology in THB materials was at first mainly used for the joining of glass. Glass welding by UF laser without the insertion of a light-absorbing intermediate layer was first reported by Tamaki et al. using 130 fs laser pulses at a low repetition rate of 1 kHz [24]. It was found that UF laser microwelding of glass successfully realized the downsizing of the welded joint, ascribed to the limitation of the thermal effect around the focal volume by the ultrashort pulse duration of the UF laser. Soon after, borosilicate glass and fused silica were joined utilizing direct interface scanning with a focused femtosecond laser [19]. A resultant weld joint with a strength of 15.3 MPa was achieved, which was the first report on UF laser microwelding of dissimilar THB materials. Since then, the range of materials suitable for UF laser microwelding has been continuously explored and expanded.

In this review paper, we overview the advances in UF laser microwelding of THB materials and THB material–metals in the past two decades, starting with the analysis of the interaction mechanisms between an UF laser and matter, and turning to the key influencing factors and practical applications of this technology. Finally, the potential future developments and research focus for UF laser microwelding technology of THB materials and THB material–metals are discussed.

2. Mechanisms of Ultrafast Laser Microwelding

UF laser microwelding of THB materials and THB material–metals belongs to a processing regime associated with extremely high light intensity. This takes full advantage of nonlinear absorption and the significantly rapid heating and cooling characteristics of UF lasers to realize microwelding by localized heat injection [25]. It is reported that, when most THB materials are illuminated by a traditional laser with VIS-NIR bands, confined electrons inside the materials cannot be excited via linear absorption to jump into the conduction band due to its intrinsic colossal bandgap [26]. Interestingly, when an UF laser

with high peak power is focused on the interface of two THB substrates, the intensity in the focal volume is sufficiently high to excite nonlinear absorption through multiphoton ionization and tunneling ionization, achieving the band gap transition of valence band electrons [27–31]. These excited, high-energy electrons further absorb photons and then, as seed electrons, can produce more free electrons through inelastic scattering, as shown in the upper part of Figure 1. This ionization process through electron collision is prone to develop into a chain reaction and then provides plenty of free electrons to the system, which is called avalanche ionization [26,32]. Half of the electrons which generate in the processes of multiphoton and avalanche ionization are reported to be immediately photoemitted from the surface and below-surface region [33]. Nevertheless, sufficient free electrons remain to be continuously accumulated at the interface by means of complex electronic transport, which creates electrostatic stress and thus initiates the Coulomb explosion. These charge dynamics of irradiated materials by UF laser are strongly associated with the absorption characteristics for each of the materials (metal, dielectrics and semiconductors) and eventually result in the formation of a high-density plasma that is localized in a small focal volume. The high-temperature plasma transfers the electron energy to the material lattice through electron–phonon coupling. The material in the vicinity of the plasma region melts or even evaporates due to thermal diffusion. Subsequently, plasma mixing and cooling, accompanied by irreversible thermal expansion of the melt, occurs at the interface around the focal volume [15,34]. After resolidification, the two substrates will be joined together.
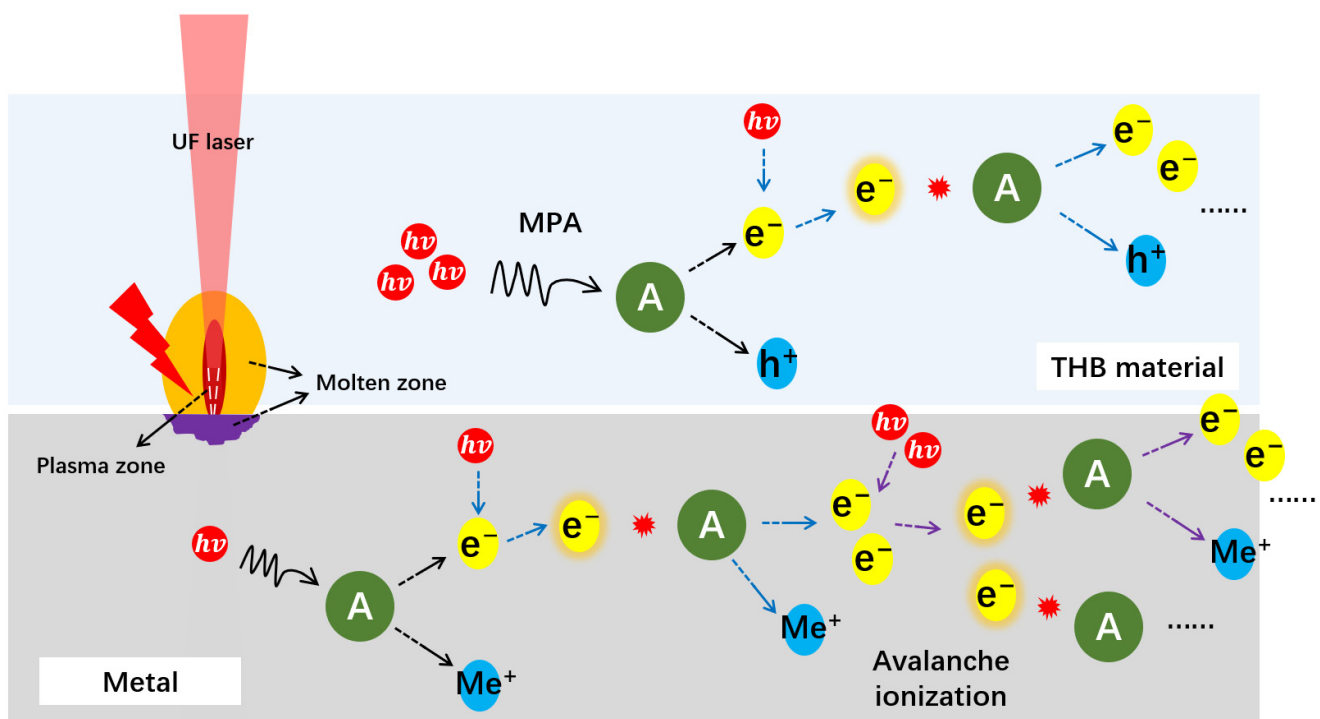

Figure 1. Schematic diagram of energy deposition process of UF laser welding THB materials and metals.

When joining THB material–metals, the metal substrate containing a large number of free electrons goes through material thermalization initiated by linear absorption (see the lower part of Figure 1), differing from the nonlinear absorption process within the THB material partner. Subsequently, electron–electron and electron–phonon scattering and lattice thermal conduction occur and result in the formation of a highly constrained plasma and melts. When the material temperature reaches the thermodynamic critical temperature, a phase explosion occurs, leading to a significant amount of high-temperature

and high-pressure metal vapor and melts. These vapors and melts ejected around the beam focus are mixed and fill the gap between the two substrates, which is required to obtain a reliable, heterogeneous weld joint [35]. Plenty of ejected melts will also be attached to the opposite THB material substrate and then transmit heat across the gap, resulting in the heating of the THB materials. If the incident energy is sufficiently high, the melt or soften zone of the THB materials will be sufficiently well developed to synergistically bridge the gaps in the micro-welds of THB material–metals [16,36]. This soften zone, together with metal melts, are subsequently cooled down, forming a weld region.

The joining mechanism is closely related to the material combination. According to the root cause of joint formation, it can be divided into mechanical interlocking at the interface between two substrates caused by thermal expansion, the mixing of plasma and molten pool, molecular diffusion, creation of chemical bonding and the hybrid mechanism. For THB material–THB material joining, Cvecek et al. [2] demonstrated that glass joining was achieved by a 10 ps laser irradiation at the energy density of 0.4 to 1.6 J/m^2, where Van der Waals forces provided by the gap bridging of bulging hot glass melt, as well as chemical bonds, were necessary. For THB material–metal joining, Zhang et al. [36] showed that copper, aluminum and stainless steel were bonded to alumina–silicate glass by femtosecond laser irradiation and considered micron/nanoscale metal particles produced by laser ablation as the adhesive, improving the interface bonding of heterogeneous joints. For welding of the two joined partners that can react with each other, reduction of silica glass was observed in the weld zone of Al and fused silica glass, which involved the formation of nanocrystalline Si and two transitional alumina phases, specifically γ- and δ-Al_2O_3 [37].

3. Advances in Ultrafast Laser Microwelding of THB Materials and THB Material–Metals

3.1. THB Material Microwelding

It is reported that a reliable, strong bonding by UF laser irradiation is affected by several factors, such as repetition rate, pulse number, pulse duration, pulse energy, focal position, the contact state of two substrates, and material combinations [16,35,38]. The change in the process parameters significantly influences the interaction between UF laser and matter, as well as the process of laser energy deposition, thus determining the behaviors of material melting, the formation of a welded joint and the resultant joint strength [39]. Hence, the influence of these factors on the microwelding of THB materials has been the focus of extensive research, which will be discussed below.

3.1.1. Pulse Repetition Frequency

The early work in joining THB materials mostly used a high-power, low-repetition-rate laser system to form a solid bonding. An amplified Ti:sapphire laser system producing 85 fs, 800 nm, 1 kHz pulses was used by Watanabe et al. to join a borosilicate glass to fused glass and the maximum joint strength was 15.3 MPa [40]. In this low-repetition-rate regime, the modified region thermalizes early and completely dissipates the energy from the previous pulse before the next pulse is delivered, as shown in Figure 2A. For a high-repetition-rate regime, the pulse period is less than heat dissipation time, resulting in the creation of thermal accumulation by laser pulse superposition, i.e., material temperature increases along with increasing laser pulses (see Figure 2B). While the thermal accumulation threshold is practically related to the material species, this dissipation process commonly occurs at the order of microseconds, which means that the required repetition rate is in the order of kHz. For silica glass and borosilicate glass, this heat dissipation time can be estimated at around 1 μs to 2 μs, which corresponds to the boundary of two regimes of around 1 MHz to 500 kHz, respectively [14].
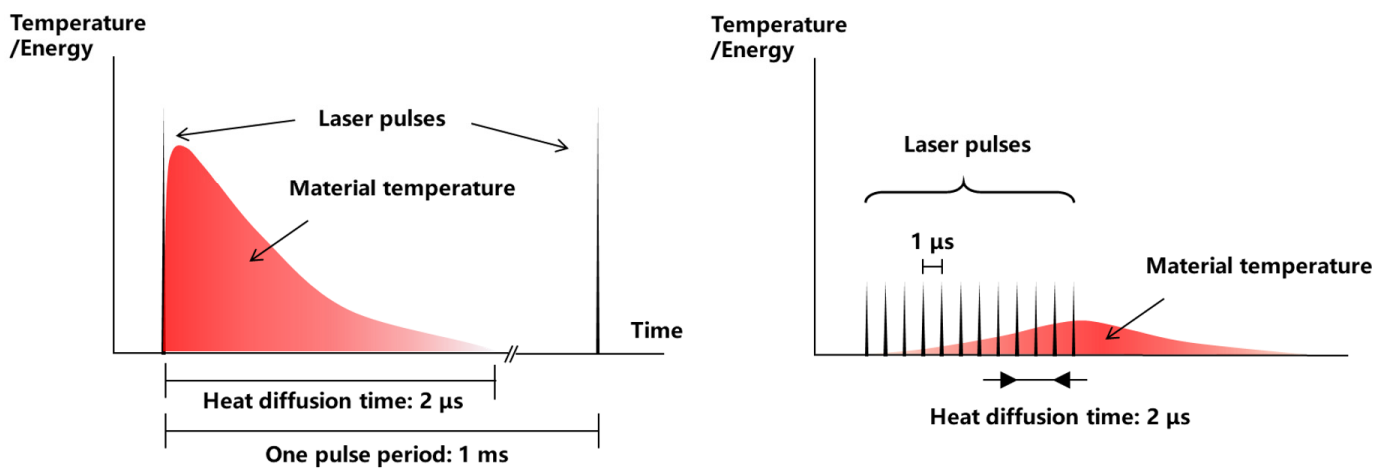
Figure 2. Energy deposition behaviors at (**A**) a low repetition rate (e.g., 1 kHz) and (**B**) a high repetition rate (e.g., 1 MHz).

Although it is possible to obtain a strong bonding in a low-repetition-rate regime, rapid and effective welding is generally dependent on thermal accumulation from multiple pulses at high repetition rates [18,35,38,40]. This is particularly true where non-ideal matching between two substrates results in a microscale gap. The accumulated heat from multiple pulses can produce a larger melted pool outside the focal volume. The resultant larger melt volume will flow into and fill the gap, contributing to the subsequent welding process. Hence, the high-repetition-rate laser system was increasingly used to join THB materials, especially for UF laser microwelding under non-optical contact conditions [41].

Miyamoto et al. [38] demonstrated the superiority of high-repetition-rate regimes for fusion welding of glass. Figure 3 shows the experimental result of irradiated borosilicate glass with a 325 fs laser at different traveling velocities using 100 kHz and 1 MHz repetition rates and the corresponding nonlinear absorptivity. The results showed that the modified zone at the repetition rate of 1 MHz was more obvious than that at the same traveling velocity at a 100 kHz repetition rate, as shown in Figure 3a. By numerical calculation, it was found that, at a higher repetition rate, the increased temperature of the irradiated region provided avalanche ionization with numerous seed electrons by thermal excitation, resulting in a two-fold growth of the nonlinear absorptivity despite the lower single pulse energy (see Figure 3b). This high absorptivity explains the rapid and effective nature of high-repetition-rate UF laser microwelding.

3.1.2. Pulse Number

Ascribed to Jee's incubation model, the ablation threshold decreases with the number of applied pulses [42]. Pulse number directly determines the amount of energy injected and its corresponding type of material modification, eventually influencing the joint formation and fusion behavior at the material interface. Chen et al. [43] presented the evolution of the plasma region and melt zone with increasing incident pulses in the fused silica glass sample in order to improve the understanding of UF laser microwelding of THB materials (see Figure 4).
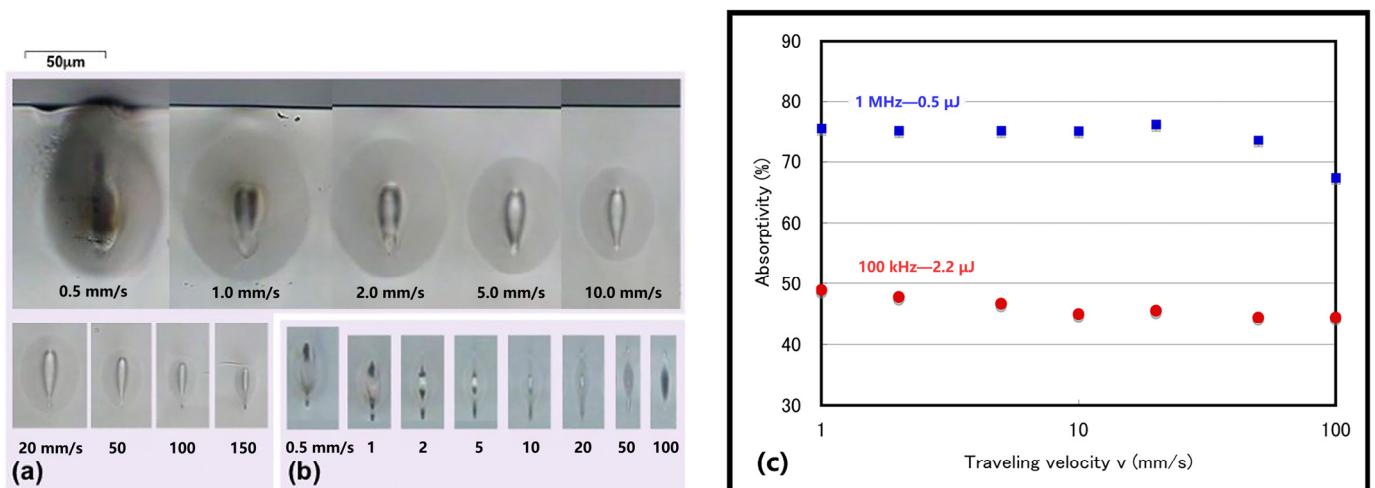
Figure 3. (**a**) Cross sections of irradiated borosilicate glass with femtosecond laser at different traveling velocities and repetition rates. (**a**) 1 MHz–0.5 µJ and (**b**) 100 kHz–2.2 µJ; (**c**) Nonlinear absorptivity of borosilicate glass dependent on traveling velocity. Reprinted from Ref. [38] with permission of Elsevier, 2016.
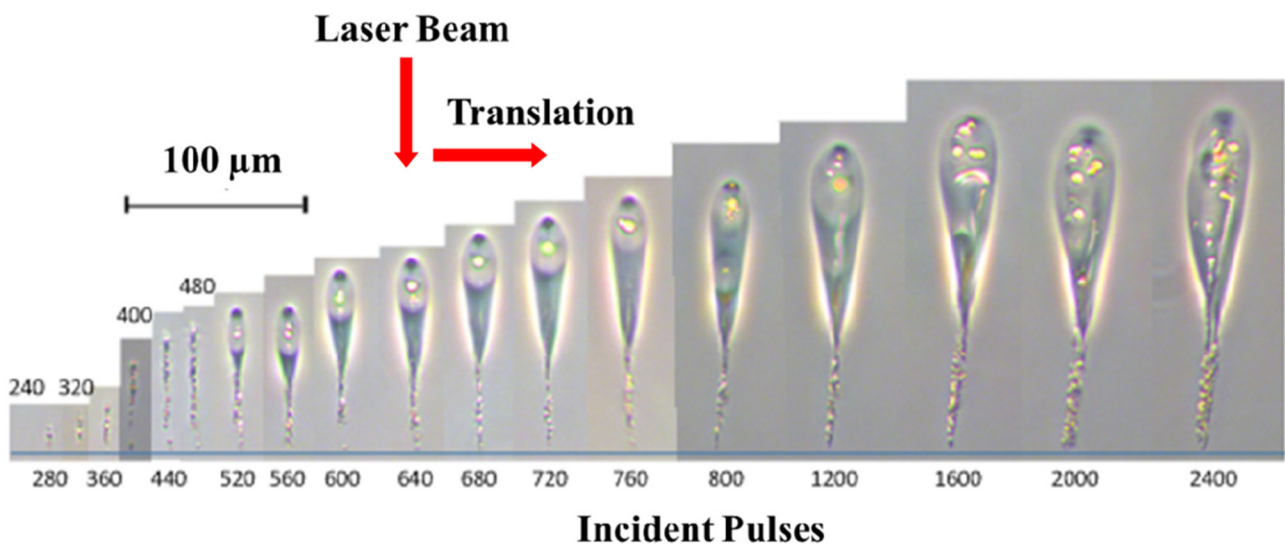

Figure 4. Evolution of laser modified region in fused silica glass with increasing number of incident pulses. Reprinted from Ref. [43] with permission of Optica Publishing Group, 2015.

The general process is as follows: the first pulses were initially absorbed within the focal volume through the nonlinear absorption process mentioned above, which offered the glass no permanent modification, but with a temperature increase around the laser focus. This increased temperature resulted in the creation of a micro-plasma cavity, with a limited melt zone surrounding it, through phonon-assisted absorption. The plasma, limited around the focal volume, was elongated with increases in the incident pulses along the laser beam axis. When the incident pulses reached a certain value (more than 280 pulses), an evident laser filamentation was observed inside the glass sample. Filamentation naturally refers to the laser pulse propagation accompanied by plasma luminescence propagation [14]. When the laser power is larger than the critical power for self-focusing, this laser will propagate through a Kerr medium, such as fused silica, and a catastrophic collapse is expected to be observed at a finite distance [44]. In fact, this collapse can be prevented by the creation of free carriers that decrease the refractive index [45]. Then, a dynamic balance between self-focusing and photoionization results in laser filamentation. Subsequent pulses are more

efficiently absorbed and the top surface of the plasma cavity was shifted upward, closer to the laser source, due to the plasma shielding effect. As the elongation of the plasma cavity continued (more than 520 pulses), lateral expansion occurred due to uneven absorption of longitudinal energy resulting from laser reflection, refraction and absorption by plasma [46]. Until the plasma rose to a certain height, the laser power density could not maintain the formation of plasma and the process terminated (around 2000 pulses). Eventually, a teardrop-like structure containing a microscale plasma cavity and the surrounding melt zone was produced after sufficient thermal relaxation.

The influence of the introduction of extra pulses (i.e., pulse train/burst mode) on THB material microwelding was also studied. Sugioka et al. [47] achieved microwelding of glass substrates using a pulse train consisting of two pulses with controllable delay time resulting from the laser temporal shaping technique, as shown in Figure 5. The results indicated that the utilization of a double-pulse train for glass welding enabled improvement in the efficiency of electron excitation and laser absorptivity, thus resulting in a higher welding velocity. With an optimized repetition rate and number of pulses in the burst, not only did this process produce a comparably large molten volume at a regime of lower applied power, but it also induced less stresses [48], which explained well the higher bonding strength of the sample prepared by a double-pulse train than that of irradiation with a conventional single-pulse train.
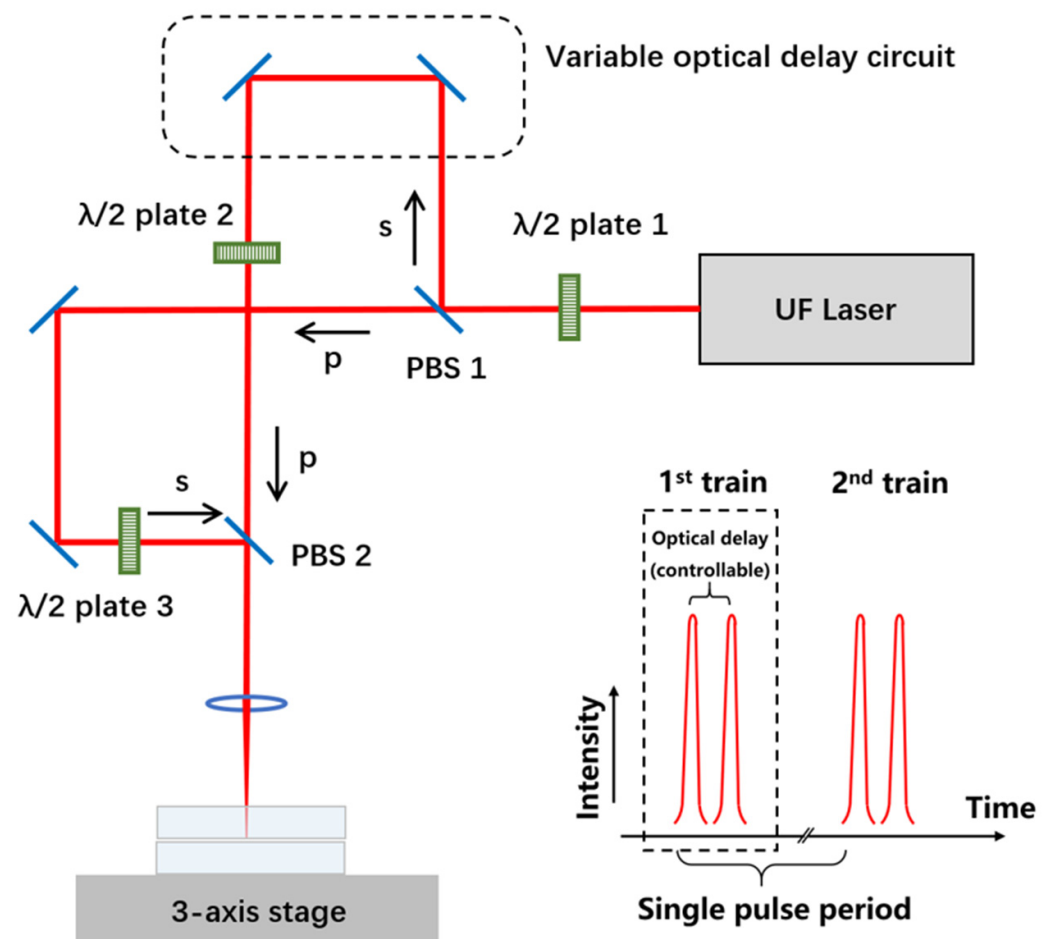

Figure 5. Schematic diagram of optical circuit setup to output a double-pulse train.

Recently, a new method of double-pulse microwelding of THB materials has been proposed to optimize the efficiency of laser energy deposition and the resultant joint performances. At the heart of this technology is the introduction of two types of lasers into

the same optical processing path. As an example, a nanosecond laser beam was introduced in the femtosecond laser glass microwelding, as described in Ref. [48]. This method should be distinguished from pulse train/burst mode. The latter is based on time-domain shaping technologies of the UF laser, where all output pulses are derived from the same seed laser. For the former, two consecutive pulses come from different seed sources, which means that the second pulse is independent of the first one and its exposure parameters can be freely set and even wholly distinct from the first pulse. Hence, this double-pulse parallel processing technology combines the characteristics of the high processing efficiency of the nanosecond laser, the non-thermal characteristics of the UF laser and pre-/post-treatment effects. Yet this technology remains in the initial stage and few investigations have been made into parallel laser microwelding of THB materials.

3.1.3. Pulse Duration

Pulse duration, as an essential parameter of the laser, determines the duration of the interaction between laser and matter, directly impacting the laser energy deposition. Herein, the characteristic time of electron–phonon coupling (τ), commonly in the order of 10 ps [29,30], is taken as a demarcation in discussing the influence of pulse duration on laser energy deposition.

For conventional lasers, i.e., continuous wave lasers and long pulse lasers (with a >100 ps pulse width), since their pulse duration is more than τ, the photon absorption is accompanied by electron–phonon coupling and phonon–phonon coupling, which efficiently enhance the thermal effects during the laser processing. Although the existence of thermal effects induced by large pulse width is beneficial to some extent for material melting, huge thermal effects also allow the workpieces to develop severe residual stress after resolidification, leading to the worsening of the joint strength. Additionally, the excessive pulse width cannot effectively excite the nonlinear absorption of THB materials, due to the inadequate peak power intensity produced by pulse compression technologies. In this case, the seed electrons provided for avalanche ionization come from lattice defects and impurities rather than multiple-photon ionization, where extra transitional energy levels between the valence band and conductive band will be introduced to facilitate the excitation of free electrons [49]. This dramatically limits the energy deposition efficiency of conventional lasers during THB material micro-welding, due to the dependence of this nonlinear absorption process on defect/impurity density.

As for the UF laser, its lower pulse duration allows for better energy deposition efficiency and weld quality, despite an attenuated welding velocity, which can be overcome by process optimization. Interestingly, with the pulse duration down to the picosecond range, the thickness of melting and the recast layer cannot be reduced to zero value even if the pulse duration is further reduced, due to the apparent optical distortion effects [42]. With a careful balancing of the influence of pulse width on the weld quality and welding efficiency, a picosecond laser can be an optimized tool for joining the THB materials. Figure 6 details the melt diameter as a function of the number of incident pulses for both femtosecond and picosecond lasers. For the same number of pulses, the pulse duration in the picosecond regime had a better energy coupling and thus led to a relatively sizeable molten region. This means that picosecond lasers have a larger, effective processing window and, because of the larger melt zone, this method is capable of joining samples with non-ideal matching (e.g., non-optical contact condition). This could simplify the sample pre-treatment procedures and improve welding efficiency. Notably, this advantage was more significant at a relatively large number of incident pulses.
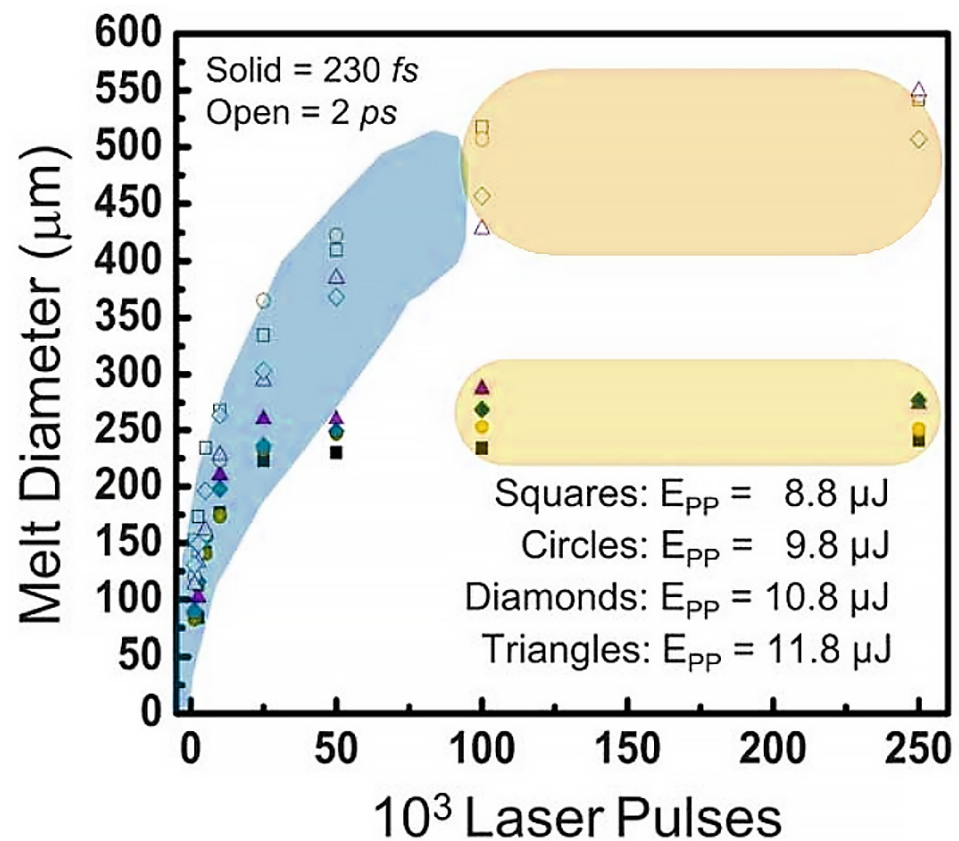
Figure 6. Dependence of melting diameter inside a transparent alumina ceramic sample on number of pulses for 2 ps and 230 fs lasers. Reprinted from Ref. [50] with permission of American Association for the Advancement of Science, 2019.

3.1.4. Pulse Energy

Microwelding dominated by laser ablation is strongly dependent on pulse energy/laser fluence. Nolte et al. indicated that two ablation regimes exist in the process of UF laser ablation of copper, both exhibiting logarithmical dependence on the laser fluence [51]. Plasma dynamics are also affected by laser fluence. At a low or moderate fluence, plasma tends to absorb most laser irradiation and plays the role of plasma shield. With laser fluence continuously rising, plasma may become transparent to the laser. Meanwhile, concomitant pressure and shockwaves improve laser energy deposition [52]. In summary, pulse energy/laser fluence can influence the process of laser energy deposition and determines the modification mechanisms of the material by laser, thus influencing the viability and efficiency of THB materials microwelding.

Figure 7a shows the correlation of nonlinear absorptivity of glass samples with pulse energy for different pulse repetition rates. With increasing pulse energy, a significant increase in nonlinear absorptivity was observed, which caused a significant expansion of the modified area, as shown in Figure 7b. This is another cause of the expansion of the modified zone, in addition to heat accumulation [25]. Therefore, heightening laser power provides an excellent solution to the issue of low energy deposition efficiency, conducive to improving material mixing and thus obtaining a strong bonding. However, excessive pulse energy will result in the deterioration of the joint formation. This brings severe thermal effects that are harmful to the achievement of a weld joint with excellent optical transmittance (see Figure 7c). The damage caused by excessive energy deposition is also reflected in the reduction of fracture toughness. Figure 7d indicates that, at the same initial crack length, the tensile fracture toughness did not monotonically enhance with single-pulse energy; instead, an optimized pulse energy occurred, beyond which the fracture toughness of welded samples diminished due to the severe thermal damage imposed.
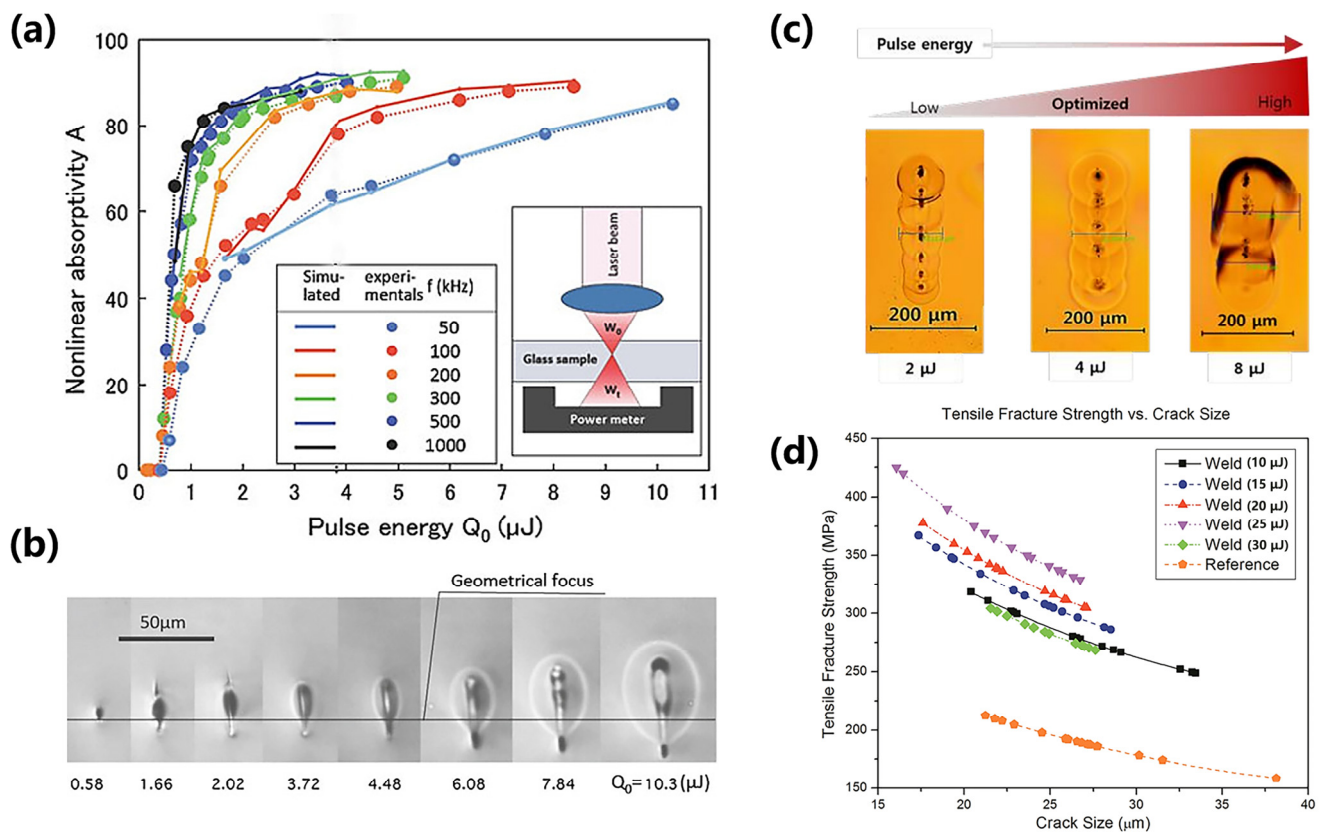
Figure 7. (**a**) Dependence of simulated and experimental nonlinear absorptivity of glass sample on pulse energy for different pulse repetition rates, reprinted from Ref. [25] with permission of Springer, 2013; (**b**) Cross sections of corresponding welded samples at constant pulse repetition rates (50 kHz) and different pulse energies, reprinted from Ref. [25] with permission of Springer, 2013; (**c**) Morphology of quartz wafer weld seams with different pulse energies, reprinted from Ref. [22] with permission of MDPI, 2019; (**d**) Fracture strength as a function of crack size of borosilicate glass weld samples at different laser energies, reprinted from Ref. [53] with permission of ASME, 2015.

Interestingly, it is observed in Figure 8a,b that, with the increase in pulse energy, an upward shift of the modified region occurred and excessive pulse energy even led to the ablation on the upper surface and the resultant plasma, consistent with the observation of Yu et al. [54]. This was due to the generated plasma, which effectively prevented the downward propagation of laser energy through the inverse bremsstrahlung absorption of plasma. This enabled the plane in the upper glass substrate, corresponding to the nonlinear absorption threshold, to continuously approach the laser source. With the increase in pulse energy, this effect was more intense and the modified zone moved further away from the focal plane, which was harmful to achieving a successful weld joint at the interface between two substrates. Hence, it is necessary to achieve a strong bonding through a synergy of multiple welding parameters [7,19].

An acceptable relationship between different parameter combinations and joint quality was investigated. Figure 8c shows the dependence of crack-free conditions upon pulse energy and pulse repetition rate in joining D263 glass. The results indicated that the formation of cracks was not solely determined by the pulse energy or repetition rate but by the result of their synergic effect. When the product of pulse energy and repetition rate exceeded the critical laser power (around 0.25 W for a 10 ps laser microwelding of D263 glass), the deposited laser energy was high enough to develop a temperature field sufficient to make the surrounding region ductile [25]. This suppressed the shrinkage stresses that cause cracks during microwelding of THB materials, making crack-free welding possible, as shown in Figure 7b.

Figure 8d indicates the thresholds of the UF laser micro-joining of borosilicate glass and fused silica as a function of the scanning speed and incident laser energy. A successful weld was achieved in region 1, whereas failed welding occurred in region 2, where the laser energy required for joining was proportional to the scanning speed. Too low laser energy and too high scanning speed caused failure to weld as a result of insufficient heat input. In region 1, higher joint strength was achieved at a higher incident laser energy and a lower scanning speed, and optimized joint strength was up to 15.3 MPa at a 12 µJ/pulse incident laser energy and a 0.1 mm/s scanning speed.
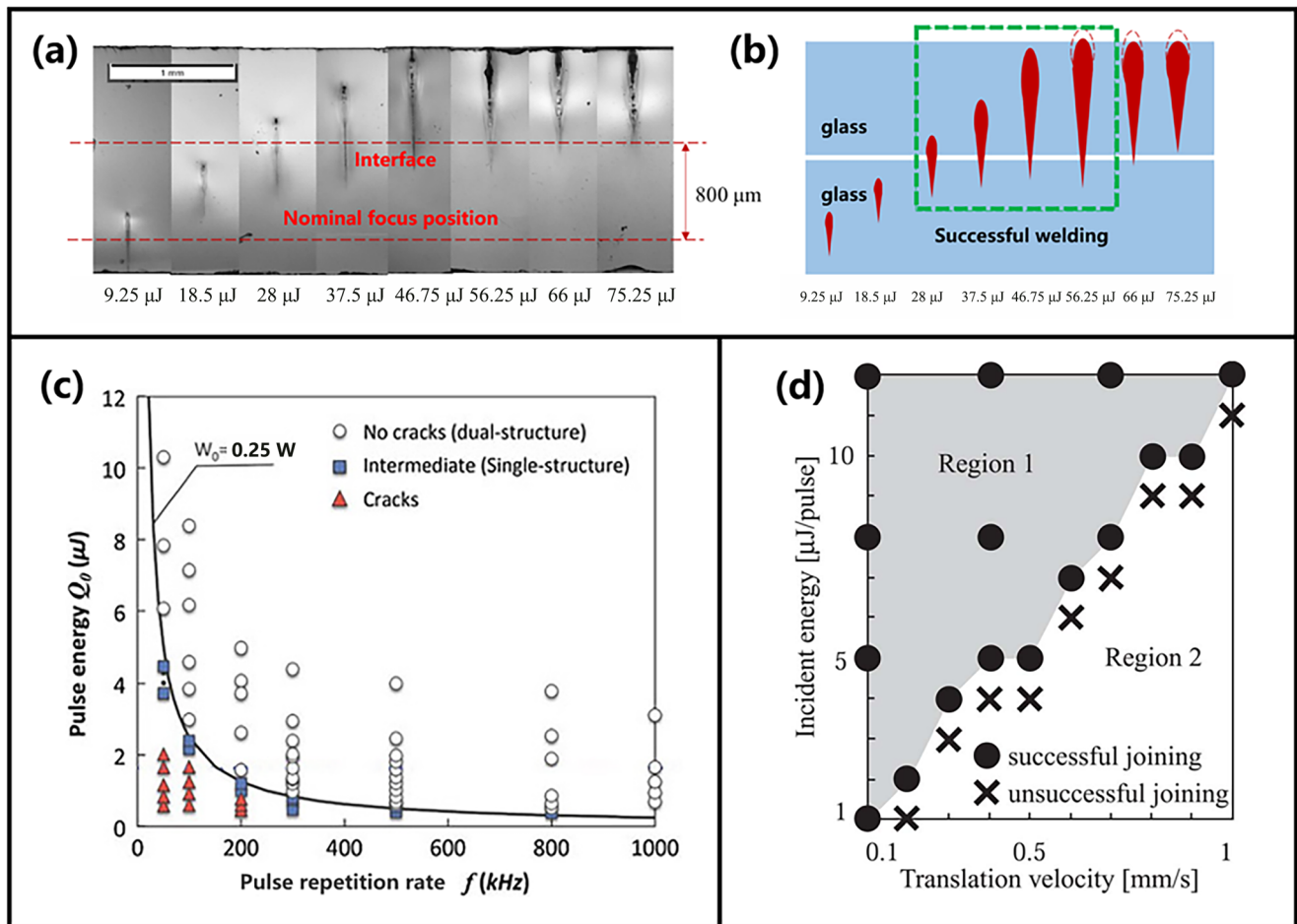

Figure 8. (**a**) Cross section of single modified glass at different pulse energies, reprinted from Ref. [55] with permission of ASME, 2015; (**b**) Schematics of glass modification at the welding regime, reprinted from Ref. [55] with permission of ASME, 2015; (**c**) Dependence of 'no crack' on pulse energy and repetition rate during UF laser microwelding of D263 glass, reprinted from Ref. [25] with permission of Spinger, 2013; (**d**) Dependence of the joining probability of borosilicate glass-fused glass on pulse energy and translation velocity, reprinted from Ref. [19] with permission of AIP Publishing, 2006.

It is concluded that consideration of the interactions between various parameters is vital in identifying the proper processing window for successful microwelding.

3.1.5. Focal Position

Since the modified region by UF laser is highly localized, which is ascribed to the nonlinear energy deposition, considerable care is required to ensure that the focal plane is accurately positioned to maintain the repeatability of a successful bonding [16,56].

Figure 9 depicts two distinct welding regimes for THB materials at different focal positions. When the focal position was significantly lower than the sample interface, only

the molten region approached the interface and the interface bulge induced by thermal expansion occurred, playing the role of mechanical bonding in joining two substrates. Since there was no material mixing, this regime achieves the non-blended welding of THB materials, which allows a clear interface surrounding the weld joint, as shown in Figure 9b. As the focal plane moved up, the laser-induced plasma region traversed the interface. In this case, the thermal bulge was replaced by the melt from the upper and lower substrates, as well as the mixed plasma ejected near the focus, which filled the material gap to obtain a reliable joint (see Figure 9d). In comparison with the former regime, the latter belongs to a blending welding regime, due to the heavy material mixing at the interface. To a large extent, this regime will impair the optical properties of welded joints.
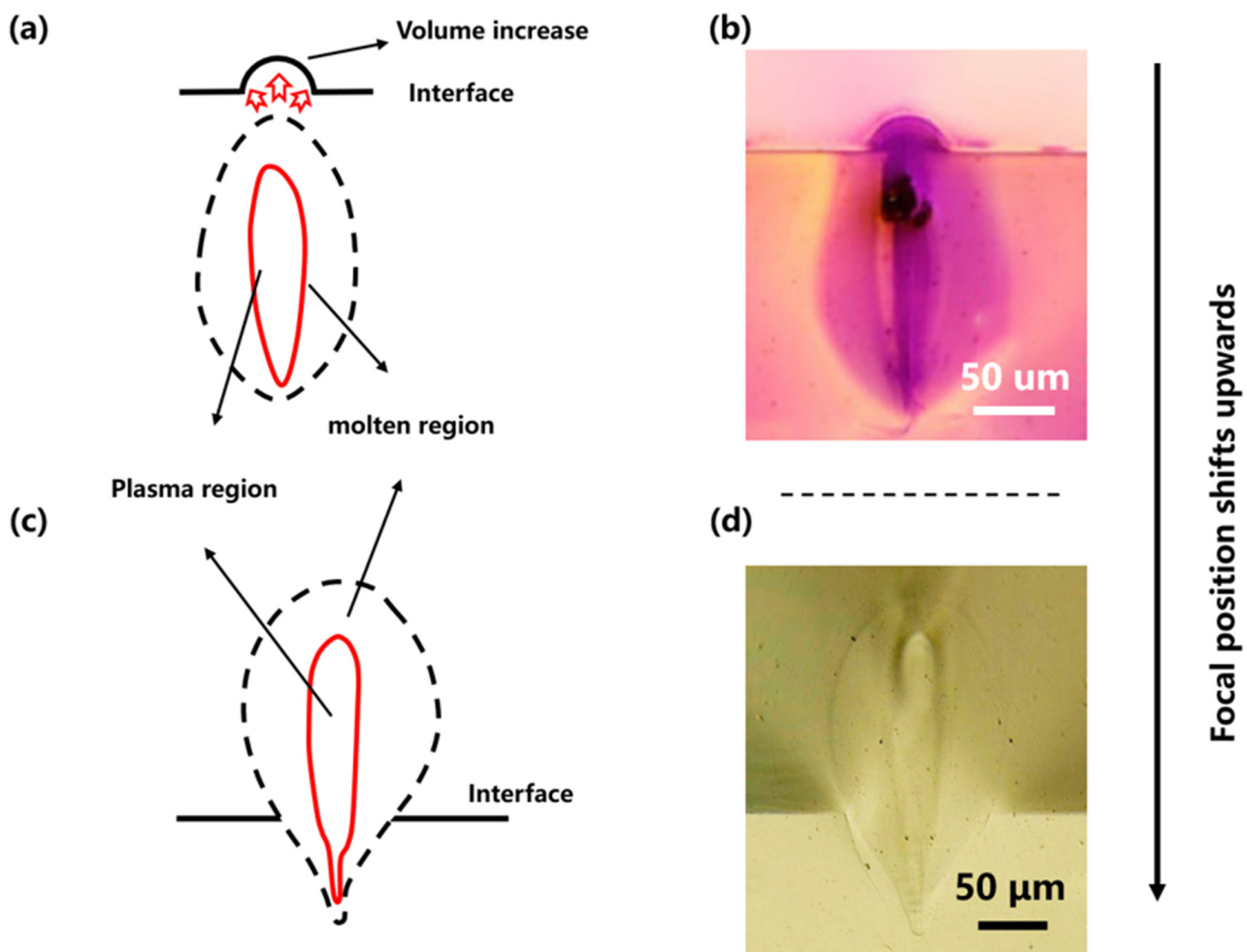

Figure 9. (**a**,**b**) Schematic diagram and cross-section image of weld seam with a focal position within the lower substrate, reprinted from Ref. [34] with the permission of Optica Publishing Group, 2015; (**c**,**d**) Schematic diagram and cross-section image of weld seam with a focal position within the lower substrate but close to the interface, reprinted from Ref. [2] with permission of Elesiver, 2010.

Different focal positions also cause a concomitant change in joint morphology and strength [7,35]. Figure 10a indicates that the weld width at the interface decreased significantly as the focal plane moved upward. Interestingly, the relationship between focal position and bonding strength was not simply proportional and there was an optimized focal position beyond which the resultant joint strength became attenuated due to the poor forming quality, as shown in Figure 10b. It is clear in Figure 10c that too high and too low a focal position caused insufficient melt to bridge the gap, thus resulting in a decreased bonding area and joint strength, which is different from the results in Figure 10a. The

inconsistency in the results is likely to stem from the too narrow range of focal positions chosen by Zhang et al. [57]. Additionally, Figure 10 also shows the downward shift of the optimized focal position corresponding to the maximum bonding strength when increasing the scanning speed. This confirms that the focal position is highly sensitive and thus considerable care is required to position the focal plane for different material and parameter combinations.
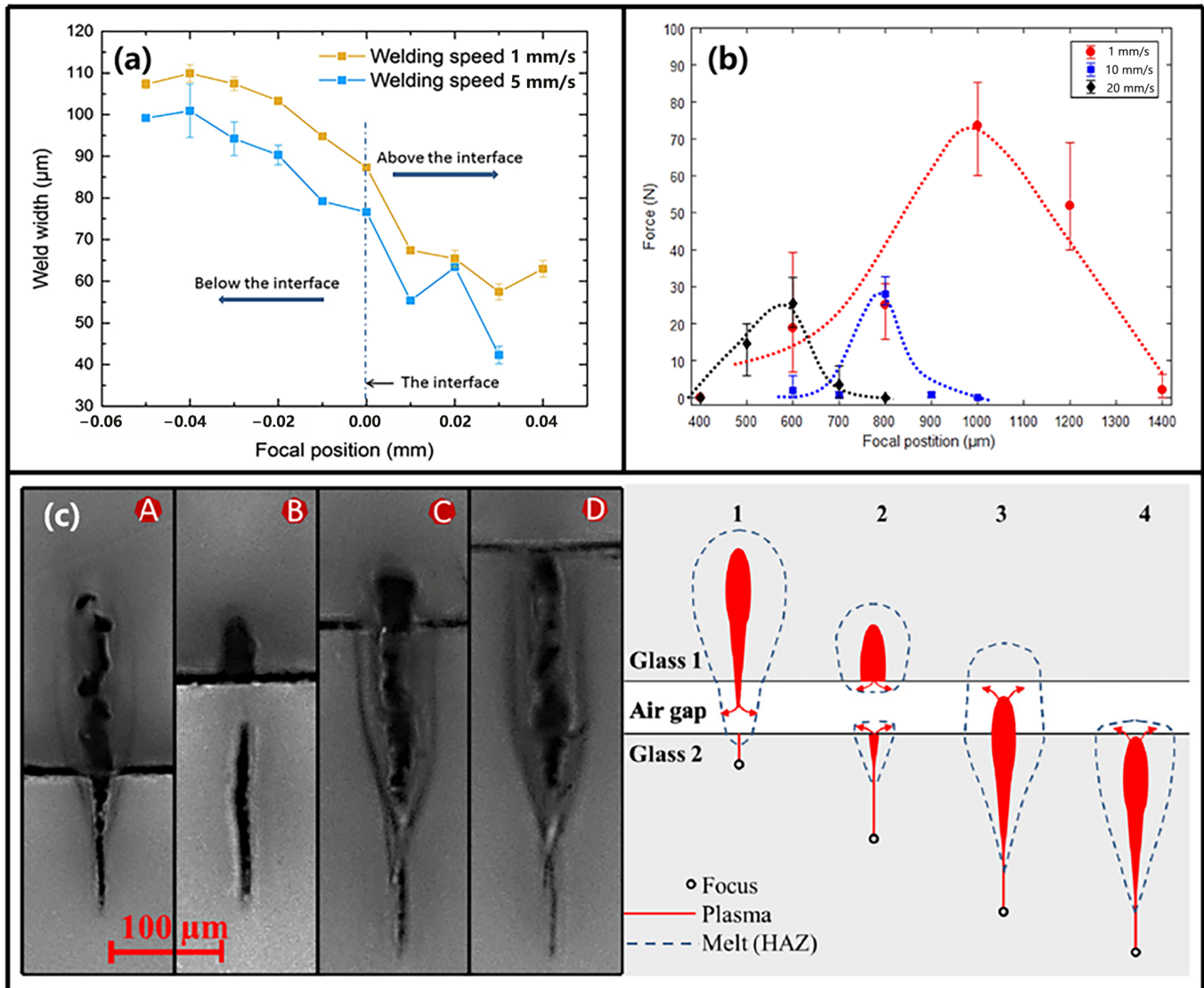

Figure 10. (**a**) Dependence of weld width of silicon-glass on focal position for scanning speed of 1 and 5 mm/s, reprinted from Ref. [57] with permission of Elesiver, 2019; (**b**) Dependence of bonding strength of fused silica glass on focal position, reprinted from Ref. [55] with permission of ASME, 2019; (**c**) Cross-sections and schematic diagrams of joined glass substrates by picosecond laser at different focal positions, reprinted from Ref. [43] with permission of Optica Publishing Group, 2015.

3.1.6. Contact States

One of the common challenges faced during ultrafast laser microwelding of THB materials is the need for pre-processing to achieve optical contact between the two substrates [43,58]. For microwelding to be successful, the plasma and splashed melt must be confined, especially during THB material–metal welding [15]. In general, this requires the two substrates to be in very close contact. In the majority of earlier studies, the gap between two samples must be below a quarter of the wavelength (i.e., optical contact) to

achieve satisfactory micro-welds. The suitability for joining could be judged by observing alternating light and dark stripes, namely Newton's ring pattern. To achieve optical contact states, it is necessary to obtain a sufficiently small surface roughness by polishing treatment, or even the use of mechanical constraints (see Figure 11) is required [17–19,40,59], which makes the pre-preparation of microwelding complex. Whilst many THB materials are available with a flatness less than $\lambda/4$ (λ: wavelength), it is easy to achieve on an interface with a large area or on a curved surface sample. Additionally, the use of a fixture or clamp to provide a mechanical constraint will also cause sample deformation or even fracture due to the applied extra pressure, which is a source of residual stress, despite reducing the gap between two substrates. This residual stress is introduced to the welding interface, causing the deterioration of mechanical properties of the welded samples, and even cracks [36,60].
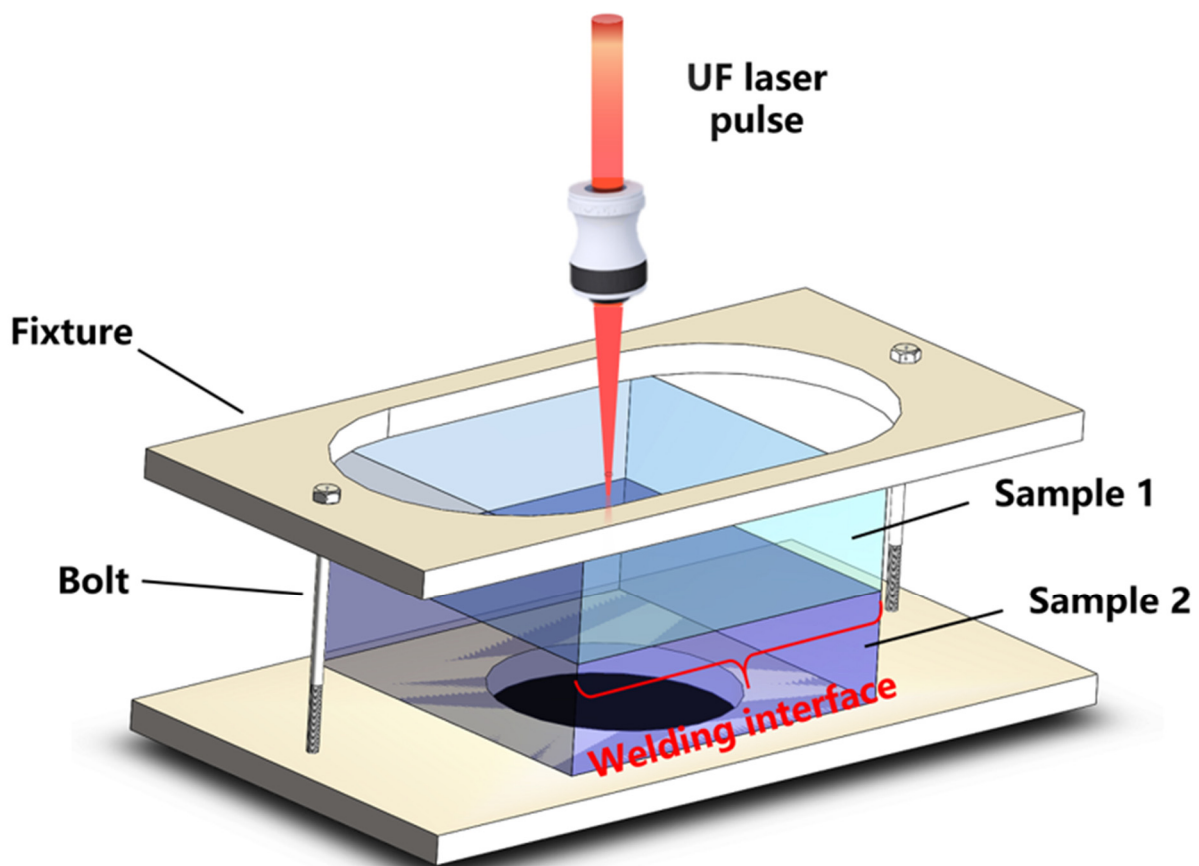

Figure 11. Schematic diagram of sample fixture for obtaining optical contact.

Numerous efforts have been made to develop UF laser microwelding of THB materials without optical contact to simplify the welding procedure [34,43,61]. As early as 2007, UF laser filamentation-assisted microwelding technology was proposed. Watanabe et al. [62] indicated the joint volume produced by the two-dimensional translation of a 30-μm-long filament region was large enough to cover the interface region during the UF laser microwelding of non-alkali glass, which provided the possibility of non-optical contact welding. Later, Cvecek et al. [34] demonstrated, for the first time, that gap filling caused by irreversible thermal bulge could be produced by UF laser microwelding of glass, which bridged the gap of approximately up to 1 μm. This method was also extended to the microwelding of different glass-type materials, including soda lime, fused silica, D263 and BF33 (see Figure 12). By optimizing the focal position of the UF laser, the maximum size of the bridged gap was increased to 3 μm [43]. Multi-scan laser welding technologies further extended this size to 5 μm and an optimized welding strength of 6.5 MPa was achieved

by Jia et al. [63]. Recently, Chen et al. [61] proposed a new method: microwelding of glasses with a 10 μm gap was achieved with small-scale rapid oscillation scanning by UF laser. These UF laser microwelding technologies indicate that optical contact is no longer essential, which is expected to facilitate their application in the manufacturing of THB material-based components.
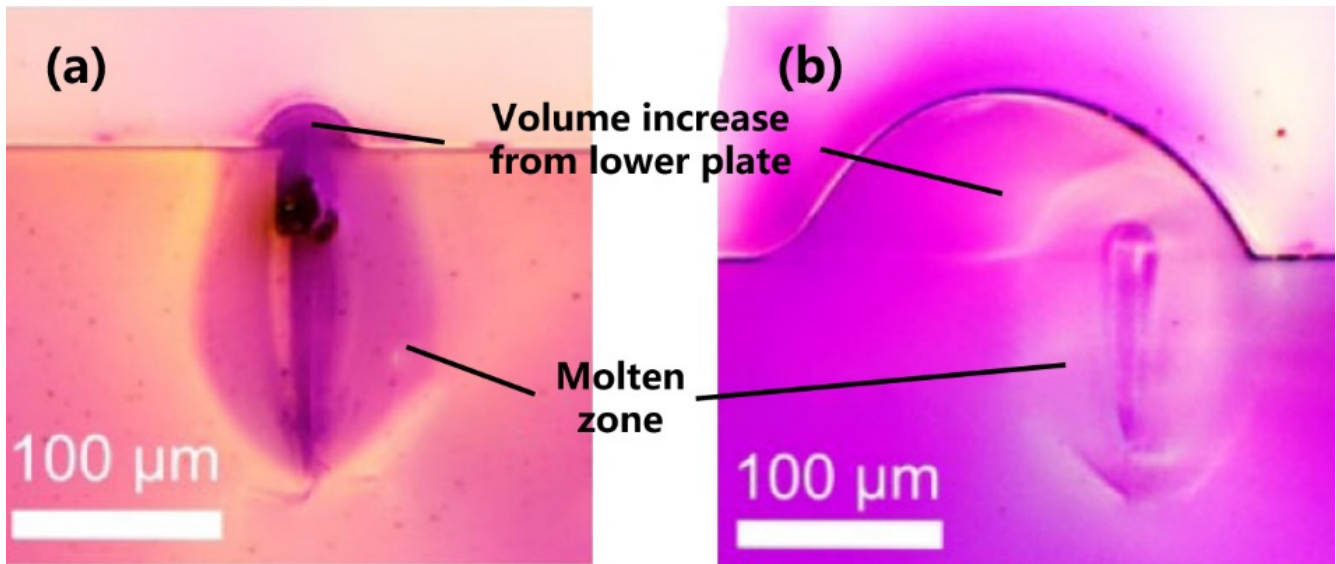

Figure 12. Cross sections of peeled-off welded joint of (**a**) BF33 and (**b**) soda lime glass. Reprinted from Ref. [34] with permission of Optica Publishing Group, 2015.

Nevertheless, the introduction of a gap between two substrates brings complexity to the positioning of the laser focus and then affects the resultant interface bonding. Chen et al. [34] investigated the viability of welding glass across a gap with a picosecond laser at different focal depths. Figure 13 shows a parameter mapping as a function of gap depth and focal position with a fixed pulse energy of 18.23 μJ and traveling speed of 2 mm/s. It found four types of weld results after welding across a gap as the focal plane and gap distance change: HAZ ablation, intermittently welded, continuously welded and HAZ under the interface.

Moreover, since the welded joints obtained by non-optical contact microwelding are bridged by ablative debris, it is possible to contaminate the sample interfaces due to material ablation and modification, which, to some extent, impairs the optical transmittance of the weld joint zone. Therefore, for applications where high optical properties are required, such as communication and sensing, one of the most cumbersome issues is to identify a proper gap between two substrates to suppress plasma and melt splashing and eventually preserve the optical properties of the base materials.

3.1.7. Dissimilar THB Material Combinations

Dissimilar THB material welding mainly involves glasses, optical crystals and transparent ceramics, in which laser energy deposition induced by nonlinear absorption is spatially controllable due to the free transmission of light along the propagation axis. Hence, the difference in thermal expansion coefficients, which severely limits the application of most common bonding technologies containing an annealing step in dissimilar THB material bonding, is no longer a difficult problem for UF laser microwelding, which is ascribed to the nature of localized treatment in close proximity to the focal volume.

Figure 14a shows the results of four successful welds of dissimilar glass combinations using an UF laser. A significant difference in melt width on two substrates was observed in the welding results of ULE-borosilicate, fused silica-borosilicate and BK7-fused silica, which was consistent with the observations of Hélie et al. [3]. This could be explained by

the mismatch in thermophysical properties of the material to be joined, which ultimately resulted in the discontinuous transition between two molten parts at the joining interface [64]. For the combination of Zerodur and ULE, this discontinuous interface transition was eliminated due to the comparable conductivity and softening point.
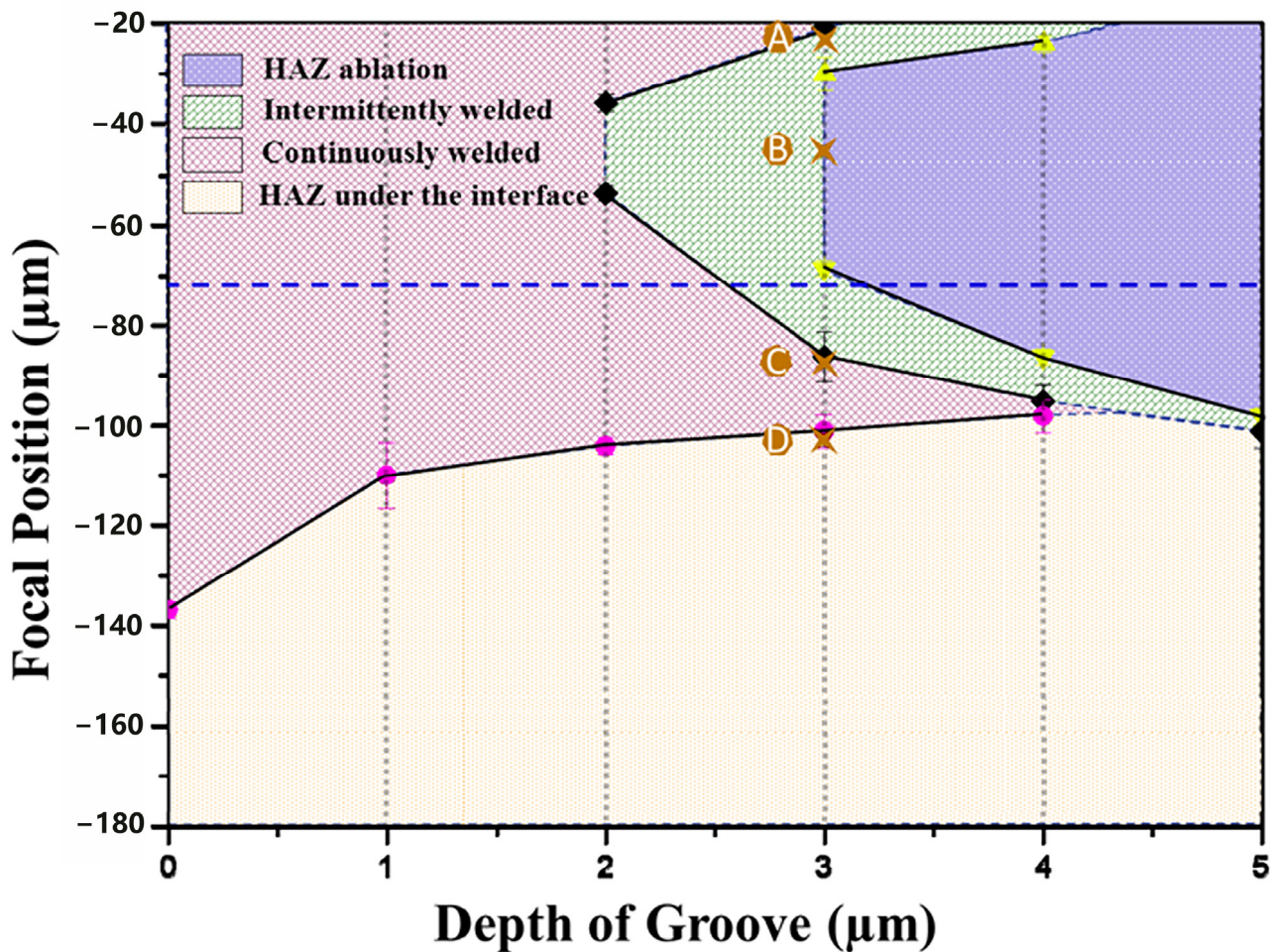

Figure 13. Classification of weld results with various parameter pairs of focal position and gap distance between two substrates. Reprinted from Ref. [43] with permission of Optica Publishing Group, 2015.

Figure 14b depicts the breaking strength of the applied base materials and the corresponding homo-/heterogeneous welded samples. These data show that the breaking strength of the base materials is the highest, followed by that of the homogeneous welded samples, and the bonding properties of the heterogeneous joints are the worst. However, the gap between the breaking strengths of homogeneous and heterogeneous joints is not significant and, in particular, the results of the dissimilar weld involving borosilicate glass even exceed the breaking strength of the corresponding homogeneous joints or base materials, as shown in Figure 14b. Thus, the great potential of UF laser for joining THB material is demonstrated.
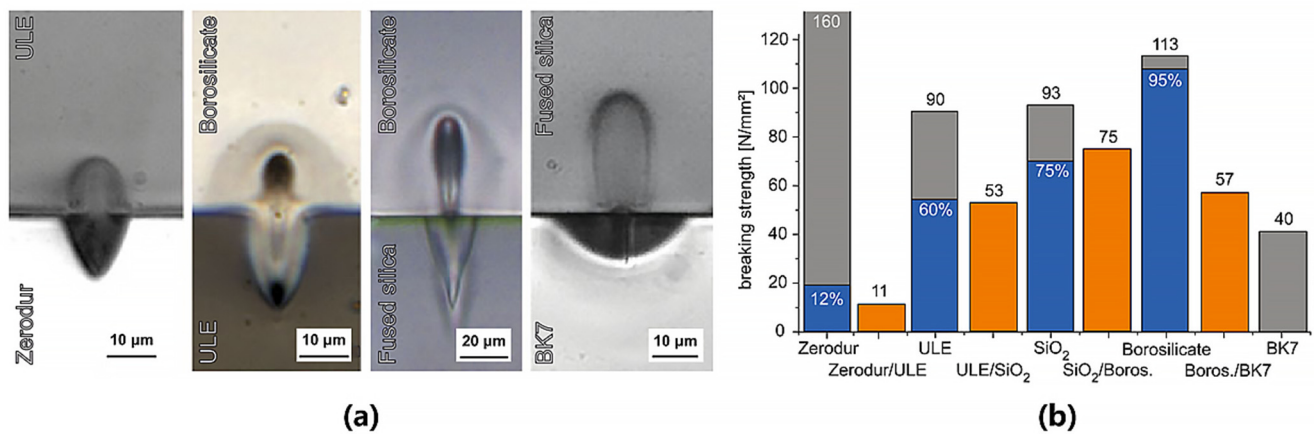
(a)

(b)

Figure 14. (**a**) Cross section of the heterogeneous weld joint of four glass combinations; (**b**) Breaking strength of welded glass samples, where the gray bars detail the breaking strength of the base material, the blue bars represent the bonding strength of homogeneous glass weld samples and the orange bars identify the welding results of dissimilar glass combinations. Reprinted from Ref. [64] with permission of Springer, 2012.

3.2. THB Material–Metal Microwelding

The success of the UF laser in applications for microwelding of heterogeneous glass by Watanabe et al. [19] aroused enthusiasm for further exploration of new material combinations suitable for UF laser microwelding. In 2006, Tamaki et al. [40] managed to achieve microwelding of non-alkali glass with silicon using a femtosecond laser with a 500 kHz repetition rate, which extended UF laser microwelding to glass-semiconductor heterogeneous material combinations. After that, Ozeki et al. [17] transplanted UF laser microwelding technology to direct welding of THB materials with metals. A strong weld joint between copper and glass without voids and cracks was obtained by a 130 fs laser and the joint strength was significantly better than those produced by nanosecond laser.

For THB material–metal welding, two distinct absorption mechanisms, together with strong interface reflection, have presented significant challenges for UF laser microwelding of THB materials with metals. Nonlinear absorption occurs in THB materials, while linear absorption takes place in metals, which makes the energy deposition process more complex and is not conducive to process optimization and quality control of the welded joints. The massive difference between two materials in physical and chemical properties also makes element diffusion at the interface, wetting and spreading, and material blending very difficult, while these processes are of great importance for obtaining THB material–metal micro-welds [35]. It was reported that, in the microwelding of 304 stainless steel and glass, the bonding strength was strongly dependent on the amount of glass wetted on the surface of the stainless steel. It is inferred that a good wetting and spreading behavior can effectively improve the joint mechanical properties [65,66]. In addition, weld cracking is another difficult issue for THB material–metal micro-welds and is easily caused by residual stress, resulting from the poor toughness of THB materials, and the significant mismatch in the expansion coefficients between the two materials to be joined. All these aspects are detrimental to constructing a strong joint with a desirable lifetime performance [16,35]. Recently, significant efforts have been made to obtain a strong bonding between THB materials and metals through UF laser microwelding.

Table 1 summarizes all the available UF laser microwelding processes of THB material–metals over the last two decades, listed from top to bottom according to publication time. It is clear that the early research mainly focused on femtosecond laser microwelding in low-repetition-rate regimes. Strong joints were obtained at the repetition rate of 1 kHz at interfaces such as glass–copper and glass–NiTi [14,17,67].

Table 1. Recent works on UF laser microwelding of THB materials with metals.

Welded Materials	Laser			Remarks	Ref.
	Pulse Width	Wave-Length	Rep. Rate		
Cu/non-alkali glass	130 fs	800 nm	1 kHz	1. optical polishing treatment and mechanical pressing; 2. successful joining without voids or cracks; 3. joint strength by fs laser: >16 MPa;	[17]
	600 ns	527 nm	1 kHz		
Cu/borosilicate	130 fs	800 nm	1 kHz	1. polishing treatment and pressure assistance; 2. joint strength: 20 MPa;	[14]
Cu/fused silica W/fused silica	70 fs	790 nm	250 kHz	1. polishing treatment and clamping assistance; 2. Cu/fused silica joint strength: 9 MPa;	[60]
NiTi/glass	35 fs	800 nm	1 kHz	1. bonding micrometric NiTi particle to glass; 2. free of cracks;	[67]
Al/SiO$_2$ Cu/SiO$_2$ SS/borosilicate SS/Sapphire	10 ps	1030 nm	400 kHz	1. polishing treatment and clamping assistance; 2. dissimilar material welding of glass and sapphire to aluminum and stainless steel has been demonstrated for the first time; 3. in all cases the welds fractured around the modified region within the glass;	[18]
Cu/Alumina-silicate Al/Alumina-silicate Steel/Alumina-silicate	160 fs	800 nm	1 kHz	1. polishing treatment and no pressure assistance; 2. Cu/glass joint shear strength: 2.34 MPa; 3. micron/nanometer-sized metal particles produced by laser ablation as adhesive;	[36]
Al/fused silica glass	5.9 ps	1030 nm	400 kHz	1. polishing treatment and clamping assistance; 2. joint formation process: nonlinear absorption, creation of plasma cavity and secondary keyholes; 3. extensive reaction was observed in the weld zone; 4. formation of nanocrystalline Si and, transitional alumina phases γ- and δ-Al$_2$O$_3$: the first time such transitional alumina phases have been reported in a laser weld;	[37]
AlSi/Nd: YAG	5.9 ps	1030 nm	400 kHz	1. polishing treatment and pressure assistance; 2. bonding of two materials with close thermal properties;	[15]
Al 6082/SiO$_2$ Al 6082/BK7	5.9 ps	1030 nm	400 kHz	1. pressure assistance and no optically polishing treatment; 2. a double-pass welding process applied; 3. parameter mapping: focal plane and incident power; 4. optimized Al 6082/BK7 bonding strength: 13 MPa;	[16]
Cu/glass	550 fs	1064 nm	1 MHz	1. no polishing treatment on metal and no pressure assistance; 2. parameter mapping: scanning speed, line interval and focal position; 3. joint shear strength: 1 MPa;	[27]

Table 1. *Cont.*

Welded Materials	Laser			Remarks	Ref.
	Pulse Width	Wave-Length	Rep. Rate		
304L SS/CaF$_2$	150 fs	780 nm	1 kHz	1. polishing treatment and pressure assistance; 2. the ablation debris solidifies and creates a bridging bond between the glass and metal surfaces; 3. significant material mixing at the interface responsible for the bond; 4. no visible gap between the CaF$_2$ and stainless steel; 5. other material combinations welded but not rigorously tested: fused silica–copper, Zerodur–Invar, fused silica–fused silica, fused silica–Zerodur, sapphire–titanium, fused silica–aluminum, sapphire–molybdenum, sapphire–Invar and diamond–Invar;	[6]
304 SS/soda lime glass	270 fs	1040 nm	400 kHz	1. surface grinding treatment but non-optical contact condition; 2. no element penetration at the junction; 3. joining mechanism: mechanical mixing, wetting and adsorption; 4. parameter mapping: pulse energy, focal position, repetition frequency and welding speed; 5. optimized joint strength: 8.79 MPa;	[35]
Al 6082/SiO$_2$	35 fs	800 nm	1 kHz	1. pressure assistance and no polishing treatment; 2. forming a mechanical pin structure consisting of adhesive regions and a concave-convex structure between two substrates; 3. shear strength: >100 MPa;	[7]
Kover/soda lime glass	300 fs	1030 nm	1 kHz	1. no polishing treatment and no pressure assistance; 2. micron/nanometer-sized metal particles condensed by plasma sprays as an adhesive part in the welding process; 3. material mixing and interdiffusion occurred; 4. shear strength: 2 MPa; 5. other material combinations welded: Cu-soda lime glass, Al6063-soda lime glass and sapphire-ceramic;	[1]
Tin powder/borosilicate glass Nickel powder/borosilicate glass Copper powder/borosilicate glass 304 stainless steel powder/borosilicate glass	350 fs	1030 nm	1.5 MHz	1. successfully and reproducibly deposited continuous tracks of powder materials on glass; 2. a relatively thin layer of approx. 3–4 μm occurring at the interface between the glass and the deposited powder; 3. an inhomogeneous material composition of the interface region 4. laser-deposited layers reaching thickness up to 60–70 μm depending on the process conditions.	[68]

Table 1. *Cont.*

Welded Materials	Laser			Remarks	Ref.
	Pulse Width	**Wave-Length**	**Rep. Rate**		
Invar 36 alloy/sapphire	800 fs	1030 nm	200 kHz	1. polishing treatment and pressure assistance; 2. successful joining without any void and microcracks; 3. welding interface consisting of a <1 μm mixed phase region with Fe-36Ni particles and sapphire; 4. bonding mechanism: chemical bonding and mechanical interlocking; 5. optimized shear strength: 108.35 MPa;	[69]

Since the welding process window was relatively narrow due to the abovementioned inherent limitations for the microwelding of THB materials with metals, most of the work was devoted to optimizing the welding process in order to achieve a strong joint on different material combinations.

Ozeki et al. [17] compared the welding results of glass–Cu joined samples by femtosecond and nanosecond lasers. The results found that the severe thermal effect of the nanosecond laser inexorably resulted in a larger molten area and impaired the weld quality. On the contrary, the precise contours between the non-irradiated and irradiated regions were observed on the sample joined by the femtosecond laser, which highlights the superiority of UF laser microwelding. In addition, lower pulse energies were required for the femtosecond pulse source to obtain strong interface bonding due to the heightened nonlinear absorption efficiency, which was two orders of magnitude lower than when using nanosecond lasers. The decreased energy input also suppressed the formation of defects caused by thermal stress that generated microcracks in THB material–metal welded samples, resulting in better joint strengths.

Carter et al. [16] conducted a detailed analysis of the result of parameter mapping in UF laser microwelding of aluminum-BK7 and found that this process was strongly dependent on the focal plane but had great tolerance to the variation in pulse energy. An optimized bonding strength of 13 MPa was finally achieved. Crucially, producing such a joint with comparable strength to the polished fs laser joints did not require the optical polishing treatment of the metal surfaces. In addition, with a suitable combination of process parameters, the bonding strength of the 304 stainless steel-glass weld reached 8.8 MPa [35].

As THB material–metal microwelding technique has advanced, the picosecond laser microwelding process and high-repetition-rate regime have generated much interest in rapid and effective welding. A larger pulse width, together with heat accumulation caused by continuous pulse impact at a high repetition rate, aggravates the thermal effect during welding, providing a higher processing efficiency for THB material–metal microwelding. Polishing treatment and pressure assistance to achieve optical contact are no longer necessary for joining THB material to metals.

Matsuyoshi et al. [27] demonstrated the superiority of a high-repetition-rate regime in joining the substrates without optical contact. In the experiment, Cu–glass microwelding using a femtosecond laser with a 1 MHz repetition rate was carried out with no pressure assistance and no surface pre-treatment work on the copper substrate, as shown in Figure 15a. Figure 15b shows the Cu–glass sample after welding and the welded sample under this regime possessed a joint strength of 1 MPa, which was comparable to the bonding strength between the glass and polished copper. After cleaving the joined sample, analysis of element characteristics was conducted using XPS. XPS data showed that the doublet peak of Cu2p1/2 and Cu2p3/2 was detected on the surface of the cleaved glass

substrate (see Figure 15c), indicating that copper was firmly attached to the glass substrate after UF laser irradiation.
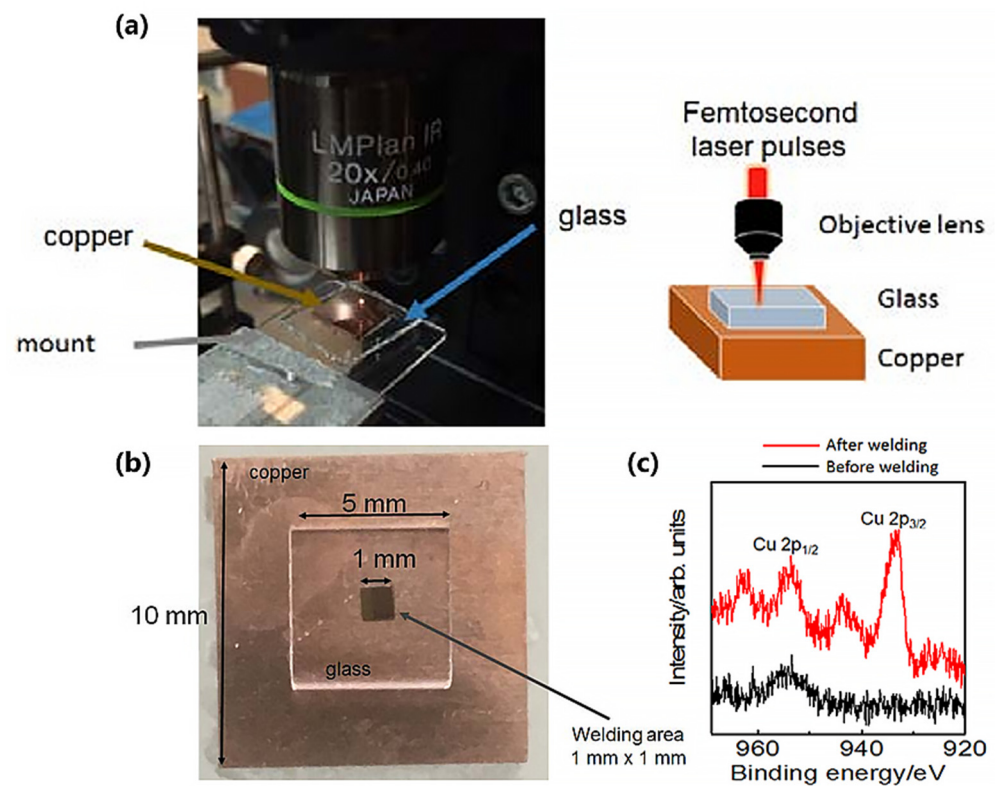

Figure 15. (**a**) Image and schematic diagram demonstrating the joining of a glass substrate to the copper plate with a rough surface by UF laser without a fixture; (**b**) Welded Cu–glass sample; (**c**) XPS spectra on the cleaved glass surface after microwelding. Reprinted from Ref. [27] with permission of JLMN, 2018.

Recently, focus has also gradually shifted from parameter mapping studies to the revelation of joining mechanisms. An increasing number of relevant research projects have started to analyze the microstructure and composition at the interface by high-end imaging/characterization instruments in order to understand the behavior of weld joint formation.

Ciuca et al. [37] investigated the microstructure and interface reaction behavior in the picosecond laser microwelding of fused silica glass and aluminum, as shown in Figure 16. The results showed that a thin interface reaction layer was generated outside the main interaction volume, where the features of a thin Si layer (see Figure 16a) and amorphous alumina consisting of dispersed ultrafine crystallites of γ- and δ-Al_2O_3 were detected (see Figure 16c,d). These metastable alumina phases were demonstrated in the welded joint containing aluminum for the first time. It was speculated that the growth of these transitional alumina phases was related to the nucleation kinetics at high supercooling, induced by picosecond high-energy-density laser pulse with a highly transient nature, resulting in the preferential formation of these phases over the equilibrium α-Al_2O_3. The appearance of nanocrystalline Si and Al_2O_3 resulting from the reduction of silica glass within the welds efficiently improved the interface bonding compared to the joint without extensive reactions. This was the first time that the occurrence of interface metallurgical behavior between THB materials and metals with widely varying chemical properties was deeply and systematically revealed, which might provide a new path towards the elucidation of strengthening and toughening mechanisms of THB material–metal weld joints.
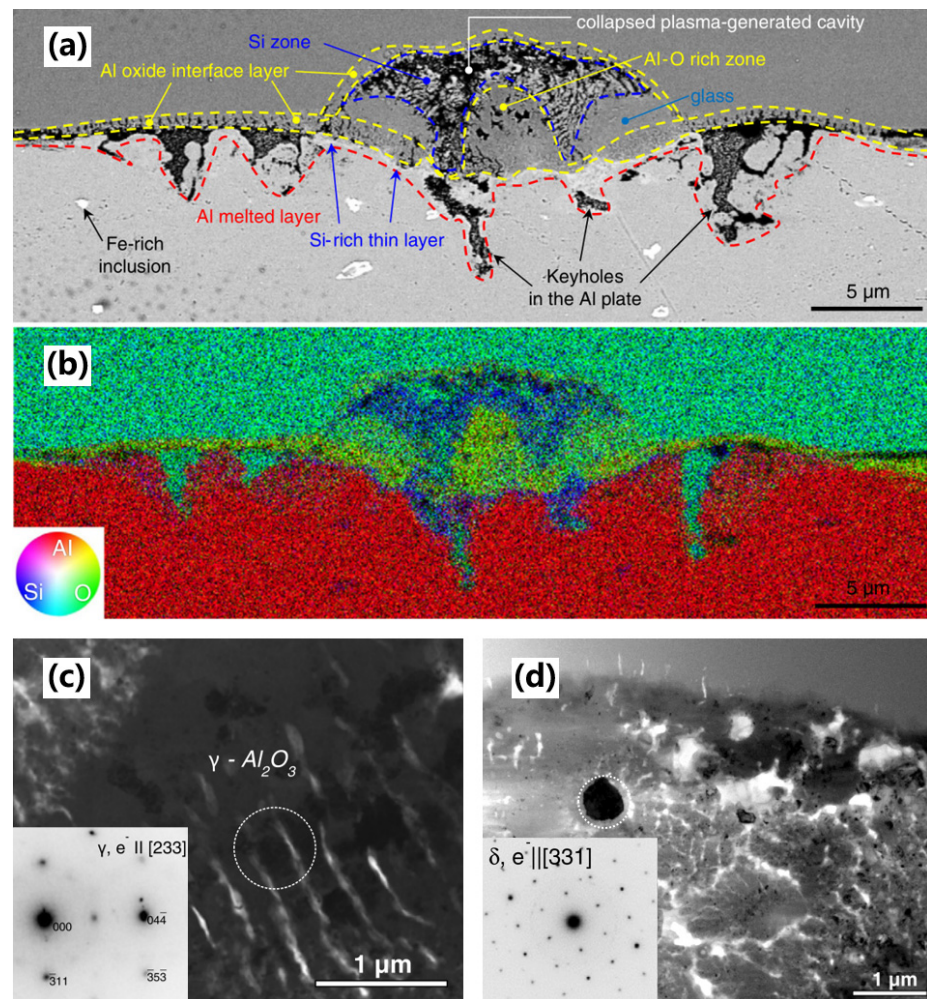
Figure 16. (**a**) Cross-section of the weld bead produced between glass and aluminum; (**b**) Corresponding EDS map of the same region; (**c**) TEM images from an Al-O rich zone close to the Al substrate, where the inset is the SADP of the area marked by the dashed circle and reveals the formation of γ-Al_2O_3; (**d**) TEM images from an Al-O rich zone close to the glass substrate, where the inset is the SADP of the dark particle marked by the dashed circle and reveals the formation of δ-Al_2O_3. Reprinted from Ref. [37] with permission of Elsevier, 2016.

Wang et al. [35] carried out 304 stainless-glass microwelding by a high-repetition-rate femtosecond laser as shown in Figure 17a and then conducted SEM characterizations for the resultant joint. An asymmetric molten zone is observed in Figure 17b and the melt on the glass side is much larger than that on the metal side. In Figure 17c, it was found that an indented interface caused by the encroachment of two molten materials occurred, which acted as a mechanical interlock to bring the two substrates together. However, for lack of further chemical component analyses, the EDS results only show the presence of a very small amount of element diffusion, as shown in Figure 17d, but insufficiently identify the special reaction products and phase composition. The author therefore argued that it was mechanical bonding rather than chemical reaction that was the joining mechanism of stainless steel and glass by fs laser irradiation. However, the analysis of fracture surface found that iron oxide was formed at the fracture surface of stainless steel, apart from the wrapping of remelted glass and convex stainless steel particles, as shown in Figure 17e,f. Wang et al. explained that the oxygen element in iron oxide was derived from the air in the gap between two substrates, which needed to be further explored, excluding the possibility of an iron element in steel bonding to oxygen in glass.
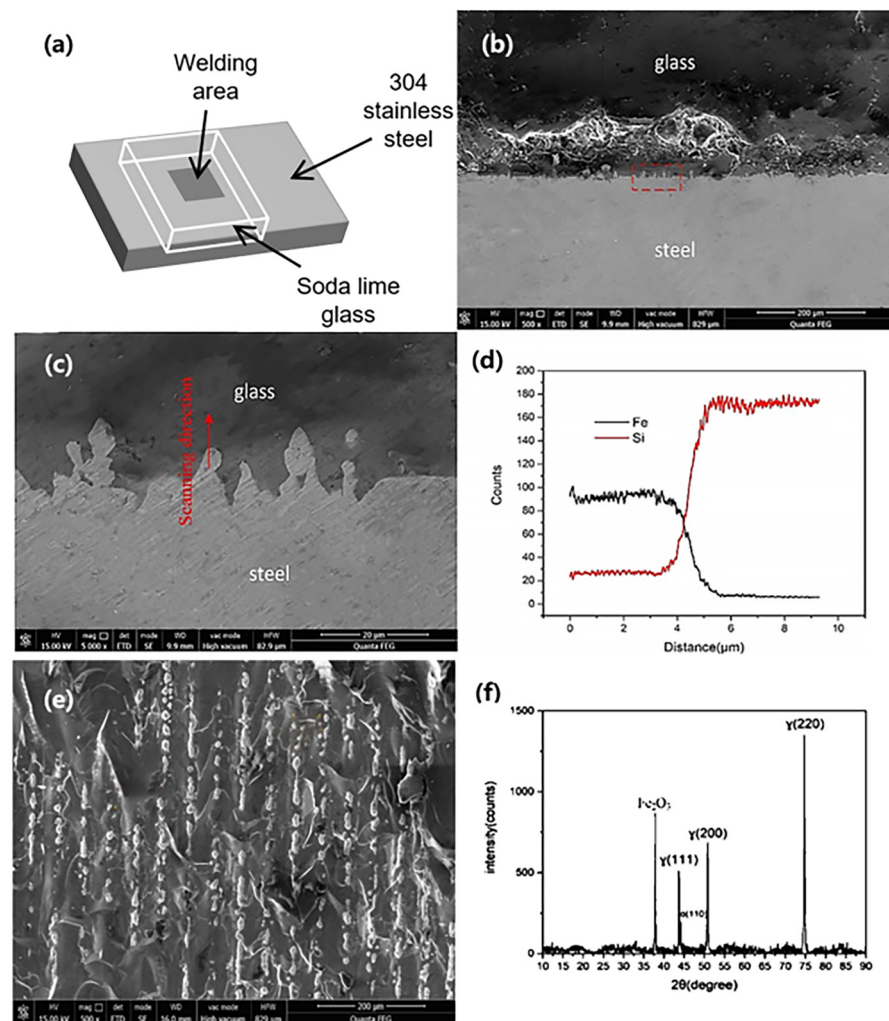
Figure 17. 304 stainless steel-soda lime glass microwelding using femtosecond laser: (**a**) Diagram of joint configuration; (**b**) SEM image of the cross-section of welded area; (**c**) Enlarged view of the red dotted square in (**c**); (**d**) Linear EDS results of the region marked in (**c**); (**e**) SEM image of fracture surface at the stainless steel side; (**f**) XRD pattern of fracture surface at the stainless steel side. Reprinted from Ref. [35] with permission of IOP Publishing, 2021.

Zhang et al. [7] experimentally identified the process window for femtosecond laser welding of Al6082-SiO$_2$ by a series of parameter mapping studies, as shown in Figure 18a. This demonstrated that, when the average power irradiated to the transparent SiO$_2$ was more than 5.5 W, the focal planes of 0.5 and 1.0 mm allowed a connection between Al and SiO$_2$ glass. When the average power was further increased to 6.4 or 7.1 W, the increase in laser power caused the formation of a larger modified region in order to allow more Al6082 to be stuck onto the SiO$_2$ substrate, which provided a wide parameter window for the focal plane. A significant tolerance of approximately 2 mm for focal positions was identified, which facilitated the achievement of a bond between the two substrates. Figure 18b shows the welding results of Al6082-SiO$_2$ at different focal positions. A pin structure caused by ablation and with some adhesive regions was observed at the interface for each focal position, which was vital for achieving a bond between Al6082–SiO$_2$. However, the rise in the focal plane resulted in a decreased ablation depth and weld width in the lower aluminum alloy substrate, which was consistent with the results of Section 3.1.5. This deterioration of joint formation might eventually cause a worse bonding strength.
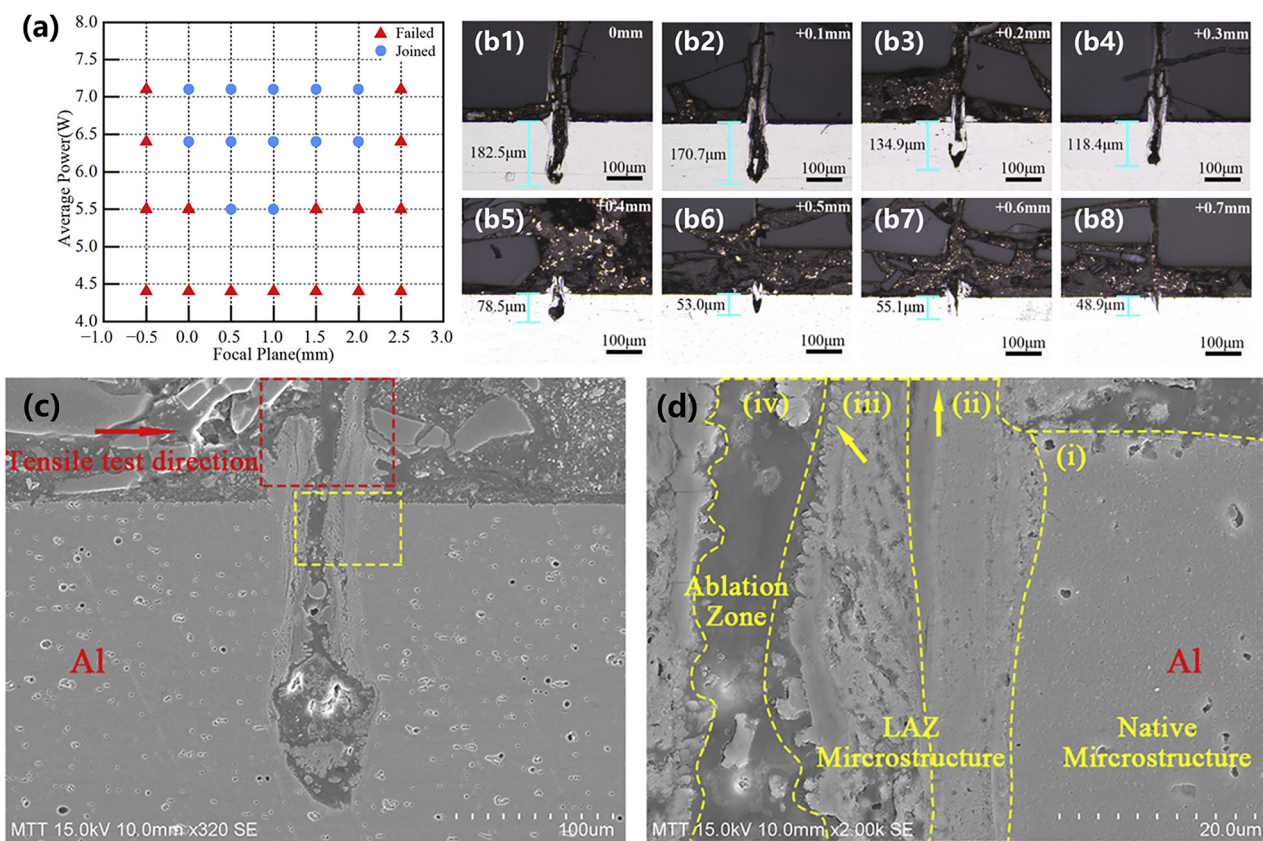
Figure 18. Femtosecond laser microwelding of Al6082 and SiO$_2$: (**a**) Dependence of the viability of joining Al6082−SiO$_2$ on laser power and focal plane; (**b1**)–(**b8**) Cross−section images of joined Al6082−SiO$_2$ at different focal positions ranging from 0 mm to +0.7 mm; (**c**) SEM images of the cross-section of the joint area of Al6082−SiO$_2$; (**d**) High magnification micrograph of the region marked by the yellow dotted square in (**c**). Reprinted from Ref. [7] with permission of Elsevier, 2022.

For an insight into the composition of the pin structure, the microstructure of aluminum-glass micro-welds was investigated, as shown in Figure 18c. At high magnification, it is clear that the pin-like weld joint at the aluminum side can be divided into four characteristic regions according to the different morphology, as shown in Figure 18d: (i) native zone, (ii) and (iii) heat affected zones and (iv) ablation zone. The microstructure of (i) and (ii) are compact, while region (iii) shows a gassy structure formed from the rapid solidification of overheated aluminum by UF laser ablation. This gassy microstructure attenuated the shear strength of the welded sample, despite the enforced bonding between two substrates by mechanical pin structure.

Ji et al. [1] achieved direct welding of soda lime glass and Kovar alloy without optical contact using a femtosecond laser. Figure 19 indicates the morphology of the soda lime glass–Kovar alloy heterogeneous joined interface. In Figure 19a, it was found that a large mass of black adherents occurred at the interface between two materials, resulting in a strong bonding effect. In addition, an irregular junction line was observed resulting from material encroachment into each other, then forming a small-sized interlock structure (see Figure 19b). To find out the element distribution within the cross-section of the glass–Kovar weld joint, surface analysis of EDS mapping was carried out, as shown in Figure 19c–f. The graph further confirms the occurrence of element diffusion during microwelding. It was speculated that there were significant interface reactions due to material mixing and element diffusion, eventually leading to the formation of a transition layer containing Fe$_2$SiO$_4$ near the bonding line that could effectively solve the mismatch of thermal properties between glass and Kovar alloy. This work provided powerful support for the challenge to the causation analysis of iron oxide in the study by Wang et al. and

broke through the conventional conception that metals and THB materials were difficult to bond together.
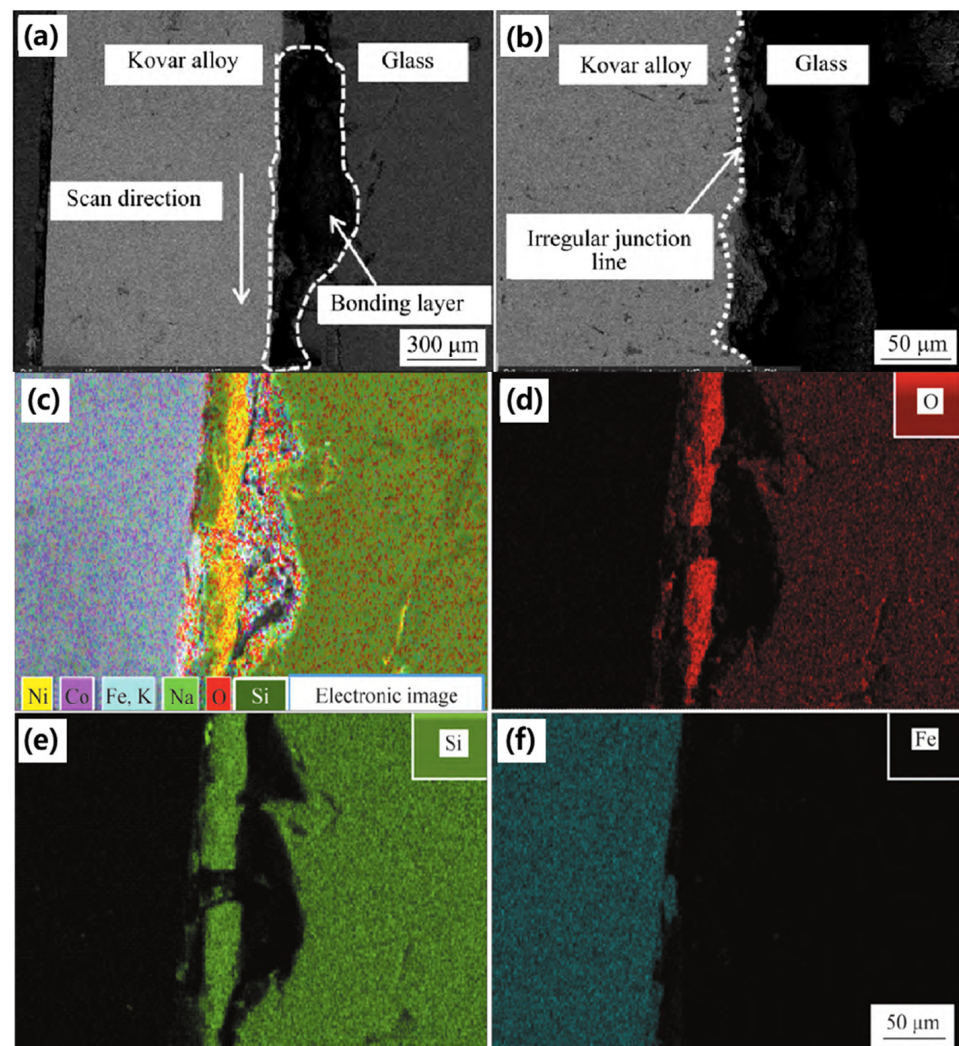

Figure 19. Cross-section of the glass–Kovar alloy micro-welds: (**a**) SEM image; (**b**) Irregular junction line at the glass–Kovar interface; EDS element mapping of (**c**) all elements and (**d**–**f**) O, Si, Fe. Reprinted from Ref. [1] with permission of Springer, 2022.

To sum up, the formation process for heterogeneous welds by ultrashort high-energy-density laser pulse is highly complicated, which is ascribed to its highly transient nature and the mismatches of thermal-physical properties between two components. There are still many thorny issues to be coped with, such as the elimination of residual stress, interface element control and the revelation of the resultant joint strengthening mechanisms. These problems significantly impact the joint quality and optical properties of samples, thus limiting the scope and progress of UF laser microwelding of THB material–metals. Although many efforts have been made in the analyses of microstructure and components at heterogeneous joined interfaces, it is impossible to adequately solve these difficult problems. To further understand joining mechanisms and to obtain successful heterogeneous welded joints, there is a need for new characterization technologies other than SEM and TEM.

Spectral tests offer the possibility of monitoring the process of ultrafast microwelding to control welding quality [70,71]. Tong et al. [72] successfully employed femtosecond laser-induced breakdown spectroscopy (fs-LIBS) as a diagnostics instrument for real-time control of the fabrication of microheater structures on thermally sprayed materials. Other spectacular demonstrations of fs-LIBS involved chemical mapping [73] and the detection

of microcracks or defects [74]. However, there have been no studies on the use of fs-LIBS technologies to monitor UF laser microwelding process. The time-resolved micro-Raman spectroscope has also proved to be an auxiliary tool for measuring temperature dynamics during UF laser micromachining, of great importance in understanding the physical nature of laser micro-processing and its modification mechanisms. By using this method, Yoshino et al. [75] studied the time- and space-dependent heat diffusion behavior around the focal volume induced by UF laser irradiation. In addition to analyzing the temperature dynamics, this spectral technique has the potential to predict the thermal stress distribution during micro-processing. Hence, we suggest that the UF laser microwelding field of spectral monitoring application should prove promising, especially in heterogeneous welding of THB material–metals with widely varying physical and chemical properties.

4. Application of Ultrafast Laser Microwelding of THB Materials and THB Material–Metals

UF laser microwelding, as an emerging precision processing technology, has attracted significant attention for the bonding of THB materials and THB material–metals, due to its high precision, high spatial selection and multi-material suitability. Nonlinear absorption enables the UF laser to join two THB substrates or THB material–metals without the assistance of a light-absorbing interlayer, which fills the gap for THB materials in multiple fields, such as electronics, communication, aeronautics and the military industry, where adhesive bonding is undesirable due to the aging and gasification of glues.

Since the UF laser microwelding process requires significantly less energy input to achieve a successful bonding than most established technologies, including anode bonding, it is highly suitable for packaging various materials/components susceptible to harsh environmental constraints and is expected to be applied in the fabrication and encapsulation of THB material-based microfluidic systems, optical components, photoelectronic devices and biosensor chips [22,50,76,77].

Figure 20a depicts ceramics encapsulation of an integrated circuit using UF laser microwelding technology and the corresponding welded samples. The resultant component preserves the optical transmittance of the base materials, which allows for vis-UF light access to optoelectronic devices through the ceramic package.

Figure 20b shows an implantable blood pressure sensor packaged by UF laser quartz glass microwelding. This packaging technique provides a minimized weld seam width, which allows a drastic reduction in sensor size. The encapsulated pressure sensor showed a good response to applied pressure and there was no gas leakage through the weld seam.

Figure 20c indicates a glass-Kovar micro-weld produced by femtosecond laser. To test its application in vacuum-seal connectors, a sealing test was carried out on the welded sample. The results showed that no change was observed in the sealing region before and after immersion in water, which showcased the good sealing performance of the welded glass-Kovar component. This component can also be used as an optical window for weapons and high power lasers [4].

Because of the UF laser's superior thermal management capability, high-precision selective laser welding of an endcap to an optical fiber was achieved by controlling the thermal effects via process optimization, as shown in Figure 20d, and the machining precision was as high as several microns. Since the heat was mainly concentrated in the focal volume, welding between the endcap and the cladding region caused no damage to the core area and airhole microstructure of fibers. The assembling of the fiber endcap provided adequate protection or sealing of the optical fiber tips in various situations and reduced the undesirable Fresnel reflection from the fiber end face.
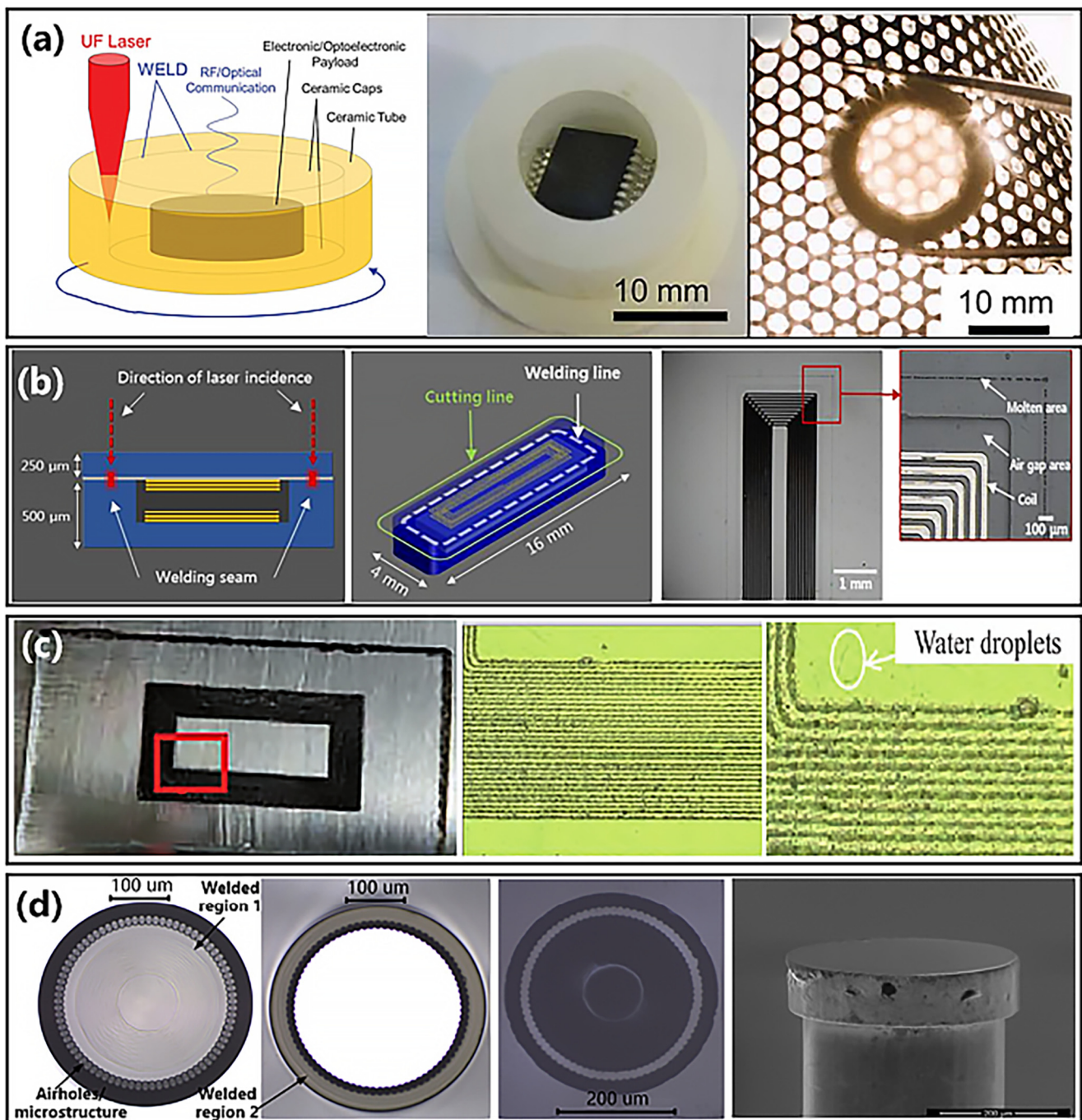
Figure 20. Application of UF laser microwelding in assembling of THB material-based components. (**a**) Encapsulation of an electronic payload with transparent ceramic tube and cap, reprinted from Ref. [50] with permission of American Association for the Advancement of Science, 2019; (**b**) Integration of an implantable blood pressure sensor, reprinted from Ref. [22] with permission of MDPI, 2019; (**c**) Vacuum-seal connector, reprinted from Ref. [1] with permission of Springer, 2022; and (**d**) Assembling of an endcap to photonic crystal fiber, reprinted from Ref. [78] with permission of Optica Publishing Group, 2013.

Through a hybrid technique containing glass etching, cutting and welding by UF laser, Jonušauskas et al. [76] successfully prepared a microfluidic system that can separate micron-sized particles of different sizes. Tan et al. [79] proposed a method to fabricate embedded thin film using picosecond laser glass welding, which offered a new idea for manufacturing thin-film devices for application in electromagnetic wave absorption. Additionally, the

threshold effect of nonlinear absorption also endows UF laser microwelding with the characteristic of spatial selectivity. This provides a possibility of UF laser direct welding of multi-layer (>2 layers) substrates [21].

Moreover, UF laser microwelding of THB materials has great potential applications in consumer electronics, such as the assembling of flexible display screens and glasses that not only protects the fragile screen from abrasive wear but also provides some unique functions, including oleo-phobicity and anti-reflection. With the rapid development of UF laser microwelding, it is certain that more potential applications in the assembling of THB material-based components will soon be developed.

5. Summary and Outlook

The energy deposition characteristics of UF lasers dominated by nonlinear absorption open up a new approach for laser-induced bonding of THB materials, which makes light-absorbing intermediate layers no longer required, efficiently simplifying the process compared with conventional laser welding technologies. However, in terms of the advances of UF laser microwelding technology, huge efforts are required to broaden the processing window and optimize the joint quality before large-scale industrial application of UF lasers for the assembling of THB material-based components. In most current works, the bonding strength of the welded joints is far less than that required for practical applications. The requirement for optical contact between THB materials has presented another major challenge for UF laser microwelding, especially in downsizing, which limits the further development of the miniaturization of microelectronics [80]. Due to the limited size of weld joints applied to device packaging, optical contact is essential to achieve such a small-sized weld joint with strong bonding, despite recent efforts in non-optical contact welding, as discussed in Section 3.1.6.

As processing technologies are continuously being iterated and updated, homogeneous welding can no longer satisfactorily meet technologically relevant applications. UF laser heterogeneous microwelding of dissimilar THB materials and THB material–metals shows great promise and is expected become the focus of extensive research shortly. However, eliminating residual thermal stresses induced by the high mismatch in thermal properties is a technical problem that must be overcome, especially in THB material–metal welding. Residual stresses will significantly affect the joint quality and optical properties, even resulting in the fracture of heterogeneous weld joints. Further optimization of welding parameters is required to achieve a strong and reliable weld joint. Recently, with the rapid development of computers and relevant technologies, finite element calculation of thermal stresses and strains opens up rich possibilities for revealing the mechanisms of residual stress formation and understanding the response of stresses to welding parameters to further diminish its influence on the properties of welded samples [81,82].

To sum up, it is suggested that future works focus on achieving high-strength joining at the interface with a microscale area or a macro larger area, especially on a curved surface sample, controlling the laser-induced localized stress, exploring the post-processing effect near the weld zone and elucidating the ultrafast plasma dynamic processes at the sample interface during microwelding. In addition, as most of the studies were carried out on the correlation between mechanical properties and welding parameters, the microstructure of weld joints has rarely been investigated until recent years, especially the heat affected zone, which has been neglected due to the limited size [23,35]. Since the microstructure near the welded joints has a close relationship with the comprehensive performances of the welded samples and reflects the weld quality, further study of the microstructural changes and the damage nucleation at the welded zone and heat affected zone is of great importance [83]. Considering the complex interaction between UF laser and matter, all the capabilities of UF laser microwelding are far from having been entirely explored. It is expected that a better understanding of the UF laser microwelding process is crucial for further scaling up of THB material application.

References

1. Ji, C.H.; Huang, Y.J.; Chen, X.; Jiang, J.Y.; Guo, Z.J.; Long, Y. Direct microwelding of dissimilar glass and Kovar alloy without optical contact using femtosecond laser pulses. *J. Cent. South Univ.* **2022**, *29*, 3422–3435. [CrossRef]
2. Cvecek, K.; Alexeev, I.; Miyamoto, I.; Schmidt, M. Defect formation in glass welding by means of ultra short laser pulses. In Proceedings of the 6th International Conference on Laser Assisted Net Shape Engineering, Erlangen, Germany, 21–24 September 2010; pp. 495–502.
3. Helie, D.; Begin, M.; Lacroix, F.; Vallee, R. Reinforced direct bonding of optical materials by femtosecond laser welding. *Appl. Opt.* **2012**, *51*, 2098–2106. [CrossRef]
4. Helie, D.; Lacroix, F.; Vallee, R. Bonding of Optical Materials by Femtosecond Laser Welding for Aerospace and High Power Laser Applications. In Proceedings of the Conference on Photonics North, Montreal, QC, Canada, 6–8 June 2012.
5. Araceli de Pablos-Martin, A.; Grosse, C.; Cismak, A.; Hoche, T. Laser-Welded Steel Foils with Sapphire Substrates. *Acta Metall. Sin. -Engl. Lett.* **2016**, *29*, 683–688. [CrossRef]
6. Lafon, R.E.; Li, S.X.; Micalizzi, F.; Lebair, S.W. Ultrafast laser bonding of glasses and crystals to metals for epoxy-free optical instruments. In Proceedings of the Conference on Components and Packaging for Laser Systems VI, San Francisco, CA, USA, 3–5 February 2020.
7. Zhang, L.; Wu, H.; Wen, J.C.; Li, M.; Shao, X.Y.; Ma, X.Q. Glass to aluminum joining by forming a mechanical pin structure using femtosecond laser. *J. Mater. Process. Technol.* **2022**, *302*, 117504. [CrossRef]
8. Overend, M.; Jin, Q.; Watson, J. The selection and performance of adhesives for a steel-glass connection. *Int. J. Adhes. Adhes.* **2011**, *31*, 587–597. [CrossRef]
9. Knapkiewicz, P.; Cichy, B.; Posadowski, W.; Tadaszak, K.; Sniadek, P.; Dziuban, J. Anodic bonding of glass-to-glass through magnetron spattered nanometric silicon layer. In Proceedings of the 25th Eurosensors Conference, Athens, Greece, 4–7 September 2011.
10. Wang, G.; Sun, X.N.; Xu, J.H.; Shan, Y.C.; Han, X.G.; Xu, J.J.; Li, J.T. Pressureless thermal diffusion bonding of transparent AlON ceramics by using a powder interlayer of parent material. *Scr. Mater.* **2019**, *171*, 118–121. [CrossRef]
11. Li, C.; Zhang, K.P.; Mao, X.J.; Si, X.Q.; Lan, B.; Liu, Z.G.; Huang, Y.X.; Qi, J.L.; Feng, J.C.; Cao, J. Microstructure and mechanical properties of the AlON/Ti6Al4V active element brazing joint. *Mater. Sci. Eng. A-Struct. Mater. Prop. Microstruct. Process.* **2020**, *793*, 139859. [CrossRef]
12. Xu, W.H.; Li, H.Y.; Yang, J.; Zhao, Y.X.; Oliveira, J.P.; Liu, H.B.; Zhang, Z.S.; Tan, C.W. Dynamic wetting and spreading mechanisms regulated by elemental Ni in a Mg/steel immiscible system during laser processing. *J. Manuf. Process.* **2022**, *80*, 600–611. [CrossRef]
13. Zheng, M.; Zhang, H.; Gao, Y.F.; Zhao, Y.X.; Tan, C.W.; Song, X.G.; Yang, J. Influence of porous high entropy alloy coating on wetting behavior and interfacial microstructure of Al-Si alloy on steel substrate. *J. Alloys Compd.* **2022**, *912*, 165154. [CrossRef]
14. Itoh, K.; Tamaki, T. Ultrafast laser microwelding for transparent and heterogeneous materials. In Proceedings of the Conference on Commercial and Biomedical Applications of Ultrafast Lasers VIII, San Jose, CA, USA, 20–23 January 2008.
15. Carter, R.M.; Troughton, M.; Chen, J.Y.; Elder, I.; Thomson, R.R.; Lamb, R.A.; Esser, M.J.D.; Hand, D.P. Picosecond laser bonding of highly dissimilar materials. In Proceedings of the Conference on Emerging Imaging and Sensing Technologies, Edinburgh, Scotland, 28–29 September 2016.
16. Carter, R.M.; Troughton, M.; Chen, J.; Elder, I.; Thomson, R.R.; Daniel Esser, M.J.; Lamb, R.A.; Hand, D.P. Towards industrial ultrafast laser microwelding: SiO_2 and BK7 to aluminum alloy. *Appl. Opt.* **2017**, *56*, 4873–4881. [CrossRef]

17. Ozeki, Y.; Inoue, T.; Tamaki, T.; Yamaguchi, H.; Onda, S.; Watanabe, W.; Sano, T.; Nishiuchi, S.; Hirose, A.; Itoh, K. Direct Welding between Copper and Glass Substrates with Femtosecond Laser Pulses. *Appl. Phys. Express* **2008**, *1*, 082601. [CrossRef]

18. Carter, R.M.; Chen, J.Y.; Shephard, J.D.; Thomson, R.R.; Hand, D.P. Picosecond laser welding of similar and dissimilar materials. *Appl. Opt.* **2014**, *53*, 4233–4238. [CrossRef] [PubMed]

19. Watanabe, W.; Onda, S.; Tamaki, T.; Itoh, K.; Nishii, J. Space-selective laser joining of dissimilar transparent materials using femtosecond laser pulses. *Appl. Phys. Lett.* **2006**, *89*, 021106. [CrossRef]

20. Richter, S.; Nolte, S.; Tunnermann, A. Ultrashort pulse laser welding—A new approach for high-stability bonding of different glasses. In Proceedings of the 7th Conference on Laser Assisted Net shape Engineering (LANE)/International Conference on Photonic Technologies, Furth, Germany, 12–15 November 2012; pp. 556–562.

21. Tan, H.; Duan, J. One-step femtosecond laser welding and internal machining of three glass substrates. *Appl. Phys. A-Mater. Sci. Process.* **2017**, *123*, 377. [CrossRef]

22. Kim, S.; Park, J.; So, S.; Ahn, S.; Choi, J.; Koo, C.; Joung, Y.H. Characteristics of an Implantable Blood Pressure Sensor Packaged by Ultrafast Laser Microwelding. *Sensors* **2019**, *19*, 1801. [CrossRef]

23. Lipateva, T.O.; Okhrimchuk, A.G.; Lipatiev, A.S.; Karateev, I.A.; Fedotov, S.S.; Lotarev, S.V.; Shestakov, A.V.; Sigaev, V.N. Robust and adhesive-free joint of Nd:YAG crystals by femtosecond laser-assisted welding. *Opt. Laser Technol.* **2022**, *146*, 107594. [CrossRef]

24. Tamaki, T.; Watanabe, W.; Nishii, J.; Itoh, K. Welding of Transparent Materials Using Femtosecond Laser Pulses. *Jpn. J. Appl. Phys.* **2005**, *44*, L687. [CrossRef]

25. Miyamoto, I.; Cvecek, K.; Okamoto, Y.; Schmidt, M. Internal modification of glass by ultrashort laser pulse and its application to microwelding. *Appl. Phys. A-Mater. Sci. Process.* **2014**, *114*, 187–208. [CrossRef]

26. Eaton, S.M.; Cerullo, G.; Osellame, R. Fundamentals of Femtosecond Laser Modification of Bulk Dielectrics. In *Femtosecond Laser Micromaching: Photonic and Microfluidic Devices in Transparent Materials*; Osellame, R., Cerullo, G., Ramponi, R., Eds.; Springer: Berlin, Germany, 2012; Volume 123, pp. 3–18.

27. Matsuyoshi, S.; Mizuguchi, Y.; Muratsugu, A.; Yamada, H.; Tamaki, T.; Watanabe, W. Welding of Glass and Copper with a Rough Surface using Femtosecond Fiber Laser Pulses. *J. Laser Micro Nanoeng.* **2018**, *13*, 21–25. [CrossRef]

28. Sundaram, S.K.; Mazur, E. Inducing and probing non-thermal transitions in semiconductors using femtosecond laser pulses. *Nat. Mater.* **2002**, *1*, 217–224. [CrossRef]

29. Rethfeld, B.; Sokolowski-Tinten, K.; von der Linde, D.; Anisimov, S.I. Timescales in the response of materials to femtosecond laser excitation. *Appl. Phys. A* **2004**, *79*, 767–769. [CrossRef]

30. Phillips, K.C.; Gandhi, H.H.; Mazur, E.; Sundaram, S.K. Ultrafast laser processing of materials: A review. *Adv. Opt. Photonics* **2015**, *7*, 684–712. [CrossRef]

31. Chen, Z.J.; Yang, J.; Liu, H.B.; Zhao, Y.X.; Pan, R. A short review on functionalized metallic surfaces by ultrafast laser micromachining. *Int. J. Adv. Manuf. Technol.* **2022**, *119*, 6919–6948. [CrossRef]

32. Tan, D.Z.; Sharafudeen, K.N.; Yue, Y.Z.; Qiu, J.R. Femtosecond laser induced phenomena in transparent solid materials: Fundamentals and applications. *Prog. Mater. Sci.* **2016**, *76*, 154–228. [CrossRef]

33. Bulgakova, N.M.; Stoian, R.; Rosenfeld, A.; Hertel, I.V.; Campbell, E.E.B. Electronic transport and consequences for material removal in ultrafast pulsed laser ablation of materials. *Phys. Rev. B* **2004**, *69*, 054102. [CrossRef]

34. Cvecek, K.; Odato, R.; Dehmel, S.; Miyamoto, I.; Schmidt, M. Gap bridging in joining of glass using ultra short laser pulses. *Opt. Express* **2015**, *23*, 5681–5693. [CrossRef]

35. Wang, Y.P.; Li, Y.; Ao, S.S.; Luo, Z.; Zhang, D. Welding of 304 stainless steel and glass using high-repetition-frequency femtosecond laser. *Mater. Res. Express* **2021**, *8*, 106523. [CrossRef]

36. Zhang, G.D.; Cheng, G.H. Direct welding of glass and metal by 1 kHz femtosecond laser pulses. *Appl. Opt.* **2015**, *54*, 8957–8961. [CrossRef]

37. Ciuca, O.P.; Carter, R.M.; Prangnell, P.B.; Hand, D.P. Characterisation of weld zone reactions in dissimilar glass-to-aluminium pulsed picosecond laser welds. *Mater. Charact.* **2016**, *120*, 53–62. [CrossRef]

38. Miyamoto, I.; Horn, A.; Gottmann, J.; Wortmann, D.; Yoshino, F. Fusion welding of glass using femtosecond laser pulses with high-repetition rates. *J. Laser Micro/Nanoeng.* **2007**, *2*, 57–63. [CrossRef]

39. Huang, S.; Chen, R.; Zhang, H.; Ye, J.; Yang, X.; Sheng, J. A study of welding process in connecting borosilicate glass by picosecond laser pulses based on response surface methodology. *Opt. Laser Technol.* **2020**, *131*, 106427. [CrossRef]

40. Tamaki, T.; Watanabe, W.; Itoh, K. Laser micro-welding of transparent materials by a localized heat accumulation effect using a femtosecond fiber laser at 1558 nm. *Opt. Express* **2006**, *14*, 10460–10468. [CrossRef]

41. Chen, H.; Rong, Y.; Huang, Y.; Wu, C. Crack suppression of glass welding by ultrafast laser without optical contact based on light modulation. *Opt. Laser Technol.* **2023**, *164*, 109466. [CrossRef]

42. Cheng, J.; Liu, C.-S.; Shang, S.; Liu, D.; Perrie, W.; Dearden, G.; Watkins, K. A review of ultrafast laser materials micromachining. *Opt. Laser Technol.* **2013**, *46*, 88–102. [CrossRef]

43. Chen, J.; Carter, R.M.; Thomson, R.R.; Hand, D.P. Avoiding the requirement for pre-existing optical contact during picosecond laser glass-to-glass welding. *Opt. Express* **2015**, *23*, 18645–18657. [CrossRef]

44. Boyd, R.W. Chapter 7—Spontaneous Light Scattering and Acousto-optics. In *Nonlinear Optics*; Boyd, R.W., Ed.; Academic Press: San Diego, CA, USA, 1992; pp. 287–324. [CrossRef]

45. Sudrie, L.; Couairon, A.; Franco, M.; Lamouroux, B.; Prade, B.; Tzortzakis, S.; Mysyrowicz, A. Femtosecond laser-induced damage and filamentary propagation in fused silica. *Phys. Rev. Lett.* **2002**, *89*, 186601. [CrossRef] [PubMed]

46. Eaton, S.M.; Zhang, H.; Herman, P.R.; Yoshino, F.; Shah, L.; Bovatsek, J.; Arai, A.Y. Heat accumulation effects in femtosecond laser-written waveguides with variable repetition rate. *Opt. Express* **2005**, *13*, 4708–4716. [CrossRef]

47. Sugioka, K.; Iida, M.; Takai, H.; Micorikawa, K. Efficient microwelding of glass substrates by ultrafast laser irradiation using a double-pulse train. *Opt. Lett.* **2011**, *36*, 2734–2736. [CrossRef] [PubMed]

48. Wu, S.Z.; Wu, D.; Xu, J.; Wang, H.Y.; Makimura, T.; Sugioka, K.; Midorikawa, K. Absorption mechanism of the second pulse in double-pulse femtosecond laser glass microwelding. *Opt. Express* **2013**, *21*, 24049–24059. [CrossRef]

49. Stuart, B.; Feit, M.; Herman, S.; Rubenchik, A.; Shore, B.; Perry, M. Nanosecond-to-femtosecond laser-induced breakdown in dielectrics. *Phys. Rev. B Condens. Matter* **1996**, *53*, 1749–1761. [CrossRef] [PubMed]

50. Penilla, E.H.; Devia-Cruz, L.F.; Wieg, A.T.; Martinez-Torres, P.; Cuando-Espitia, N.; Sellappan, P.; Kodera, Y.; Aguilar, G.; Garay, J.E. Ultrafast laser welding of ceramics. *Science* **2019**, *365*, 803–808. [CrossRef]

51. Nolte, S.; Momma, C.; Jacobs, H.; Tünnermann, A.; Chichkov, B.N.; Wellegehausen, B.; Welling, H. Ablation of metals by ultrashort laser pulses. *J. Opt. Soc. Am. B* **1997**, *14*, 2716–2722. [CrossRef]

52. Fedosejevs, R.; Ottmann, R.; Sigel, R.; Kühnle, G.; Szatmari, S.; Schäfer, F.P. Absorption of femtosecond laser pulses in high-density plasma. *Phys. Rev. Lett.* **1990**, *64*, 1250–1253. [CrossRef] [PubMed]

53. Kongsuwan, P.; Satoh, G.; Yao, Y.L. Transmission Welding of Glass by Femtosecond Laser: Mechanism and Fracture Strength. *J. Manuf. Sci. Eng.-Trans. Asme* **2012**, *134*, 011004. [CrossRef]

54. Miao, Y.; Ting, H.; Rongshi, X. Long Focal Length Green Femtosecond Laser Welding of Glass. *Chin. J. Lasers* **2020**, *47*, 0902005. [CrossRef]

55. Zhao, K.; Wang, H.; Yan, J.; Shen, H. Welding Fused Silica Glass by Picosecond Pulsed Laser With Low Numerical Aperture. *J. Micro Nano-Manuf.* **2019**, *7*, 041007. [CrossRef]

56. Richter, S.; Zimmermann, F.; Tunnermann, A.; Nolte, S. Laser welding of glasses at high repetition rates—Fundamentals and prospects. *Opt. Laser Technol.* **2016**, *83*, 59–66. [CrossRef]

57. Zhang, J.J.; Xu, S.Z.; Dong, Y.K.; Zhang, C.Z.; Li, J.M.; Guo, L.; Zhang, Q.M. Microwelding of glass to silicon by green ultrafast laser pulses. *Opt. Laser Technol.* **2019**, *120*, 105720. [CrossRef]

58. Zhang, J.J.; Chen, S.H.; Lu, H.L.; Huang, M.H.; Li, J.M.; Guo, L.; Lue, Q.T.; Zhang, Q.M. The effect of gap on the quality of glass-to-glass welding using a picosecond laser. *Opt. Lasers Eng.* **2020**, *134*, 106248. [CrossRef]

59. Lipat'eva, T.O.; Fedotov, S.S.; Lipat'ev, A.S.; Lotarev, S.V.; Shakhgil'dyan, G.Y.; Ryabov, K.V.; Sigaev, V.N. Precision Laser Welding of Silica Glass with Iron-Nickel Alloy. *Glass Ceram.* **2021**, *77*, 435–437. [CrossRef]

60. Lacroix, F.; Helie, D.; Vallee, R. Optical Bonding Reinforced by Femtosecond Laser Welding. In Proceedings of the Conference on Optical Manufacturing and Testing IX, San Diego, CA, USA, 22–24 August 2011.

61. Chen, H.; Deng, L.M.; Duan, J.; Zeng, X.Y. Picosecond laser welding of glasses with a large gap by a rapid oscillating scan. *Opt. Lett.* **2019**, *44*, 2570–2573. [CrossRef]

62. Watanabe, W.; Tamaki, T.; Itoh, K. Filamentation in laser microprocessing and microwelding. In Proceedings of the International Conference on Lasers, Applications, and Technologies, Minsk, Byelarus, 28 May–1 June 2007.

63. Jia, X.; Li, K.; Li, Z.; Wang, C.; Chen, J.; Cui, S. Multi-scan picosecond laser welding of non-optical contact soda lime glass. *Opt. Laser Technol.* **2023**, *161*, 109164. [CrossRef]

64. Richter, S.; Zimmermann, F.; Doring, S.; Tunnermann, A.; Nolte, S. Ultrashort high repetition rate exposure of dielectric materials: Laser bonding of glasses analyzed by micro-Raman spectroscopy. *Appl. Phys. A-Mater. Sci. Process.* **2013**, *110*, 9–15. [CrossRef]

65. Liu, Z.; Yang, J.; Li, Y.; Li, W.; Chen, J.; Shen, L.; Zhang, P.; Zhishui, Y. Wetting and Spreading Behaviors of Al-Si Alloy on Surface Textured Stainless Steel by Ultrafast Laser. *Appl. Surf. Sci.* **2020**, *520*, 146316. [CrossRef]

66. Li, H.; Li, L.Q.; Huang, R.; Tan, C.; Yang, J.; Hongbo, X.; Chen, B. The effect of surface texturing on the laser-induced wetting behavior of AlSi5 alloy on Ti6Al4V alloy. *Appl. Surf. Sci.* **2021**, *566*, 150630. [CrossRef]

67. Quintino, L.; Liu, L.; Miranda, R.M.; Silva, R.J.C.; Hu, A.; Zhou, Y. Bonding NiTi to glass with femtosecond laser pulses. *Mater. Lett.* **2013**, *98*, 142–145. [CrossRef]

68. Mingareev, I.; Bautista, N.; Yadav, D.; Bhanderi, A. Ultrafast laser deposition of powder materials on glass. *Opt. Laser Technol.* **2023**, *160*, 109078. [CrossRef]

69. Pan, R.; Yang, D.; Zhou, T.; Feng, Y.; Dong, Z.; Yan, Z.; Li, P.; Yang, J.; Chen, S. Micro-welding of sapphire and metal by femtosecond laser. *Ceram. Int.* 2023; *in press.* [CrossRef]

70. Labutin, T.A.; Lednev, V.N.; Ilyin, A.A.; Popov, A.M. Femtosecond laser-induced breakdown spectroscopy. *J. Anal. At. Spectrom.* **2016**, *31*, 90–118. [CrossRef]

71. Watanabe, W.; Li, Y.; Itoh, K. Ultrafast laser micro-processing of transparent material. *Opt. Laser Technol.* **2016**, *78*, 52–61. [CrossRef]

72. Tong, T.; Li, J.; Longtin, J.P. Real-time control of ultrafast laser micromachining by laser-induced breakdown spectroscopy. *Appl. Opt.* **2004**, *43*, 1971–1980. [CrossRef]

73. Hou, H.; Cheng, L.; Richardson, T.; Chen, G.; Doeff, M.; Zheng, R.; Russo, R.; Zorba, V. Three-dimensional elemental imaging of Li-ion solid-state electrolytes using fs-laser induced breakdown spectroscopy (LIBS). *J. Anal. At. Spectrom.* **2015**, *30*, 2295–2302. [CrossRef]

74. Wessel, W.; Brueckner-Foit, A.; Mildner, J.; Englert, L.; Haag, L.; Horn, A.; Wollenhaupt, M.; Baumert, T. Use of femtosecond laser-induced breakdown spectroscopy (fs-LIBS) for micro-crack analysis on the surface. *Eng. Fract. Mech.* **2010**, *77*, 1874–1883. [CrossRef]

75. Yoshino, T.; Ozeki, Y.; Matsumoto, M.; Itoh, K. In situ Micro-Raman Investigation of Spatio-Temporal Evolution of Heat in Ultrafast Laser Microprocessing of Glass. *Jpn. J. Appl. Phys.* **2012**, *51*, 102403. [CrossRef]

76. Jonusauskas, L.; Rekstyte, S.; Buividas, R.; Butkus, S.; Gadonas, R.; Juodkazis, S.; Malinauskas, M. Hybrid subtractive-additive-welding microfabrication for lab-on-chip applications via single amplified femtosecond laser source. *Opt. Eng.* **2017**, *56*, 094108. [CrossRef]

77. Fujiwara, J.; Tamaki, T. Measuring sealing degree of welded glass substrates after ultrafast laser microwelding. *Appl. Phys. A* **2022**, *128*, 1076. [CrossRef]

78. Helie, D.; Gouin, S.; Vallee, R. Assembling an endcap to optical fibers by femtosecond laser welding and milling. *Opt. Mater. Express* **2013**, *3*, 1742–1754. [CrossRef]

79. Tan, H.; Yang, W.; Huang, Q.; Pan, J.; Li, C.; Fu, X. Embedded thin film fabrication via glass welding by an ultrafast laser. *J. Asian Ceram. Soc.* **2023**, *11*, 62–67. [CrossRef]

80. Miyamoto, I.; Cvecek, K.; Schmidt, M. Advances of Laser Welding Technology of Glass -Science and Technology. *J. Laser Micro Nanoeng.* **2020**, *15*, 63–76. [CrossRef]

81. Wen, J.; Zhang, L.; Wu, H.; Li, M.; Ma, X. Molecular Dynamics Simulation of Aluminum-Fused Silica Interface Shot by Femtosecond Laser. *Laser Optoelectron. Prog.* **2023**, *60*, 0114011. [CrossRef]

82. Zhang, S.W.; Kong, M.; Miao, H.; Memon, S.; Zhang, Y.J.; Liu, S.X. Transient temperature and stress fields on bonding small glass pieces to solder glass by laser welding: Numerical modelling and experimental validation. *Sol. Energy* **2020**, *209*, 350–362. [CrossRef]

83. Xue, J.; Guo, W.; Yang, J.; Xia, M.; Zhao, G.; Tan, C.; Wan, Z.; Chi, J.; Zhang, H. In-situ observation of microcrack initiation and damage nucleation modes on the HAZ of laser-welded DP1180 joint. *J. Mater. Sci. Technol.* **2023**, *148*, 138–149. [CrossRef]